Biochemical and structural characterization of murine GBP7, a guanylate binding protein with an elongated C-terminal tail

Larissa Legewie[1], Jennifer Loschwitz[2,3], Nora Steffens[1], Martin Prescher[4], Xue Wang[2,3], Sander H. J. Smits[4,5], Lutz Schmitt[4], Birgit Strodel[2,3], Daniel Degrandi[1]* and Klaus Pfeffer[1]*

From the [1]Institute of Medical Microbiology and Hospital Hygiene, Heinrich Heine University, Duesseldorf, Germany, [2]Institute of Complex Systems: Structural Biochemistry, Forschungszentrum Juelich, Juelich, Germany, [3]Institute of Theoretical and Computational Chemistry, Heinrich Heine University, Duesseldorf, Germany, [4]Institute of Biochemistry, Heinrich Heine University, Duesseldorf, Germany, [5]Center for Structural Studies, Heinrich Heine University, Duesseldorf, Germany

*To whom correspondence should be addressed: Daniel Degrandi and Klaus Pfeffer: Institute of Medical Microbiology and Hospital Hygiene, Heinrich Heine University, Universitätsstrasse 1, 40225 Düsseldorf, Germany; daniel.degrandi@hhu.de; klaus.pfeffer@hhu.de; Tel. +49 211 811-2459; Fax. +49 211 811-5906

Keywords: guanylate binding protein, GTPase, protein purification, enzyme kinetics, dimerization, homology modeling, molecular dynamics, C-terminal domain

Abstract

Guanylate-binding proteins (GBPs) constitute a family of interferon-inducible guanosine triphosphatases (GTPases) that are key players in host defense against intracellular pathogens ranging from protozoa to bacteria and viruses. So far, human GBP1 and GBP5 as well as murine GBP2 have been biochemically characterized in detail. Here, with murine GBP7 (mGBP7), a GBP family member with an unconventional and elongated C-terminus is analyzed. The present study demonstrates that mGBP7 exhibits a concentration-dependent GTPase activity and an apparent GTP turnover number of 20 min^{-1}. In addition, fluorescence spectroscopy analyses reveal that mGBP7 binds GTP with high affinity ($K_D = 0.22$ µM) and GTPase activity assays indicate that mGBP7 hydrolyzes GTP to GDP and GMP. The mGBP7 GTPase activity is inhibited by incubation with γ-phosphate analogues and a K51A mutation interfering with GTP binding. SEC-MALS analyses give evidence that mGBP7 forms transient dimers and that this oligomerization pattern is not influenced by the presence of nucleotides. Moreover, a structural model for mGBP7 is provided by homology modeling, which shows that the GTPase possesses an elongated C-terminal tail compared to the Caa*X* motif containing mGBP2 and human GBP1. Molecular dynamics simulations indicate that this tail has trans-membrane characteristics and, interestingly, confocal microscopy analyses reveal that the C-terminal tail is required for recruitment of mGBP7 to the parasitophorous vacuole of *Toxoplasma gondii*.

Introduction

The 65-73 kDa guanylate binding proteins (p65 GBPs) belong to the interferon (IFN)-induced GTPases of the dynamin superfamily (1). Members of this superfamily utilize the energy of GTP hydrolysis to execute various structural changes, which are necessary to remodel cellular membranes or to initiate fusion events (2, 3). Several studies on GBPs demonstrated that their accumulation at membranes of intracellular pathogens is essential for host immunity (4-6). For example, GBPs have been shown to target the parasitophorous vacuole (PV) of the protozoan parasite *Toxoplasma gondii* (*T. gondii*) and the bacteria containing vacuoles of *Chlamydia trachomatis* (*C. trachomatis*), *Legionella pneumophila*, and *Francisella* spp. (7-12). However, only scarce data are available about the requirements for GTP binding, GTP hydrolysis, and oligomerization, which are essential to understand the exact mechanisms by which GBPs exert their role in host defense (7, 8, 13).

In general, the GBP family is highly conserved in vertebrates and exhibits a high degree of homology among each other. The GBP domain architecture is comprised of two parts: The N-terminal globular GTPase (G) domain and the elongated helical domain that can be subdivided into a middle (M) region, and a C-terminal GTPase effector (E) region. The G domain harbors the GTP-binding site containing four conserved sequence elements: the canonical G1 motif or phosphate-binding loop (P-loop) G*XXXX*GK(S/T), the switch1/G2 T motif, the phosphate- and Mg^{2+}-binding switch2/G3 D*XX*G sequence, and the nucleotide-specificity providing T(V/L)RD G4 motif (14). The T(V/L)RD motif deviates from the classical N/TK*X*D motif in other GTP-binding proteins (15, 16). The helical M region consists of two helix bundles (α7-11) and extends away from the G domain which gives the molecule an elongated shape (17). The C-terminal E region consists of two helices (α12/13) which folds back along the M region of the helical domain to the G domain and allows the long α12 helix to interact via eight contacts with the M region and via four contacts with the G domain (17).

To date, seven human GBPs (hGBP1 to hGBP7) and 11 murine GBPs (mGBP1 to mGBP11) have been identified (14, 18, 19). Three of these 11 mGBPs, mGBP1, -2, and -5, contain a C-terminal Caa*X* motif, which is posttranslationally modified by a farnesyl or geranylgeranyl isoprene moiety and is required for membrane interaction (7, 19-21). Until now, mainly GBPs bearing such a membrane anchoring motif have been biochemically characterized in detail (7, 22, 23). Other mGBPs lacking this particular motif, such as mGBP7, the largest mGBP family member, or its closest human relatives (hGBP4 and hGBP6) have not yet been investigated with regard to their biochemical characteristics and abilities to interact with membranes. mGBP7 was shown to be highly induced in murine cells by IFNγ and, to a lower extent, by IFNβ (18). Also, it was found to be induced in lung, liver, and spleen of *Listeria monocytogenes* and *T. gondii* infected mice, implying a significant role of mGBP7 in infection (18).

It has been reported that upon binding of GTP GBPs self-assemble into dimers which stimulates their enzymatic activity (24, 25). The dimerization of GBPs has been reported to be established through contact between two G domains (20). This dimerization induces the positioning of a conserved arginine residue of the P-loop toward the γ-phosphate and stimulates its cleavage by stabilizing the transition state of GTP hydrolysis (26). A recent quantum mechanics/molecular mechanics study revealed that S73 is also highly important for the hydrolysis reaction, which involves transfer of a proton from the water nucleophile to a non-bridging phosphoryl oxygen after activation by a composite base consisting of S73, E99, a bridging water molecule, and GTP itself (27). S73 is introduced into the active site of hGBP1 only upon dimerization (27). For the unique feature of the majority of GBPs to be able to hydrolyze GTP consecutively to GDP and on to GMP, the β-phosphate in the GDP-bound form has to move to the position where the γ-phosphate is located in the GTP-bound form (7, 26, 28-30). The physiological function of this unique feature of GBPs to hydrolyze GDP is not known so far. However, the product ratio varies from 0% GMP (hGBP5 and mGBP5) up to 85-90% GMP (hGBP1) for different GBPs and experimental conditions (1, 13, 24, 31, 32). Besides the nucleotide-dependent self-assembly, further common characteristic properties of GBPs are their high intrinsic GTPase activity with turnover numbers between 2 to 102 min^{-1} and their ability to bind agarose-immobilized GMP, GDP, and GTP with µM affinities (33, 34).

Taken together, the biochemistry of GBPs as well as their structure requires further investigation to link their biochemical properties and mode of action to their biological function in host defense. In this respect, data for mGBP7 have been missing up to now. In this study, the GTPase activity of mGBP7 and a hydrolysis deficient mGBP7 mutant (K51A) is characterized. In addition, the oligomerization pattern of mGBP7 and the K51A mutant in the presence of different nucleotides is analyzed and the products of the GTP hydrolysis reaction are determined. Finally, computational modeling is used to predict the structure of mGBP7 and confocal microscopy experiments are performed to elucidate the biological function of the elongated C-terminal tail of mGBP7.

Experimental procedures

Chemicals

All chemicals for protein purification and GTPase activity measurements were ordered from Sigma if not otherwise stated. Components and chemicals used for SDS-PAGE and BN PAGE were obtained from Thermo Scientific.

Expression constructs

The WT open reading frame (ORF) of mGBP7 (NCBI accession number NM_001083312.2) was cloned into the pQE-80L plasmid (Qiagen). Site-directed mutagenesis (QuikChange II XL Site-Directed Mutagenesis Kit, Agilent Technologies) was carried out for the generation of the GTPase deficient mutant K51A. The K51A mutant was introduced into mGBP7 using forward primer 5′-

AGGACTATACCGTACGGGAGCATCCTACTTGATGAACCGC-3′ (Metabion) and reverse primer 5′-GCGGTTCATCAAGTAGGATGCTCCCGTACGGTATAGTCCT-3′ (Metabion). The sequences of both constructs were verified by DNA sequencing (Beckman Coulter Genomics).

The mGBP7 ORF (NCBI accession number NM_001083312.2) without the last 147 base pairs (mGBP7$^{\Delta49}$) was amplified by PCR using forward primer 5’-ATTCCCGGGAGCATCTGGTCC-3’ (Metabion) and reverse primer 5’-ATTCTTCTCCTTATTTAGTTGAATC-3’ (Metabion). The corresponding clones were subcloned into the pWPXL plasmid (Trono Lab (35)) as N-terminal GFP fusion constructs. WT GFP-mGBP7 and GFP-mGBP7$^{\Delta49}$ sequences were verified by DNA sequencing (BMFZ, Duesseldorf, Germany) and used for lentiviral transduction.

Transformation of E. coli

mGBP7 expression constructs were transformed into Rosetta^{TM} 2(DE3)pLysS competent cells (Novagen) using standard procedures (Novagen). The Rosetta^{TM} 2 host strain was choosen to enhance the expression of eukaryotic proteins that contain codons rarely used in *E. coli*.

Protein expression and purification

For large scale expression, a volume of 6 liters of selective 2YT medium (1.6% (w/v) tryptone, 1% (w/v) yeast extract, 0.5% (w/v) NaCl) was inoculated with 150 mL of an *E. coli* Rosetta^{TM} 2(DE3)pLysS overnight culture. The expression of WT and the K51A mGBP7 mutant with N-terminal His$_6$ tag were induced by adding 150 μM isopropyl-β-D-thiogalactopyranoside (IPTG) at an A_{600} of 0.5. During both steps, the temperature was set at 37 °C and the mixer was set at 1800 rpm. After 4 h of incubation, cells were harvested by centrifugation (8000 rpm, 20 min, 4 °C) and resuspended in high salt buffer (50 mM Tris-HCl, 5 mM $MgCl_2$, 300 mM NaCl, 10 mM imidazole, 1 mM β-mercaptoethanol, 250 μM Pefabloc (Roche), pH 8). Bacteria were disrupted by multiple passes through a cell disrupter (Constant Systems) at 2.7 kbar. After centrifugation for 1 h at 48000 rpm, 40 mL of the supernatant was added to 10 mL of equilibrated Ni-NTA resin suspension (Qiagen) and incubated overnight on a rotary shaker (200 rpm) at 4 °C. After three washing steps with 45 mL low salt buffer (50 mM Tris-HCl, 5 mM $MgCl_2$, 250 mM NaCl, 10 mM imidazole, 1 mM β-mercaptoethanol, pH 8) mGBP7 and the mGBP7 K51A mutant were eluted with 5 mL of high imidazole buffer (50 mM Tris-HCl, 5 mM $MgCl_2$, 150 mM NaCl, 300 mM imidazole, 1 mM β-mercaptoethanol, pH 8). The 5 min centrifugation steps to sediment the Ni-NTA suspension were performed at 4 °C and 1500 rpm. Protein purity was verified by Coomassie blue stained SDS PAGE and immunoblotting. The 5 mL elution fraction was applied to a Superdex200 26/60 column (GE Healthcare) equilibrated in gel filtration buffer (50 mM Tris-HCl, 5 mM $MgCl_2$, 2 mM dithioerythritol). Fractions containing monomeric mGBP7 were pooled and concentrated using centrifugal ultrafiltration devices with a 50 kDa MWCO (Merck). 5 mL of concentrated protein was again used for a SEC run and eluted protein fractions were analyzed by Coomassie blue stained SDS

PAGE and immunoblotting. mGBP7 fractions were concentrated up to 10-20 mg/mL using 50 kDa MWCO centrifugal ultrafiltration devices, aliquoted, and stored at -80 °C.

Immunoblotting and SDS-PAGE analysis

All SDS-PAGE and Western blotting experiments were performed with standard laboratory techniques. For immunoblotting a polyclonal anti-mGBP7 antibody (Eurogentec), a monoclonal anti-Tetra His antibody (Qiagen) and a monoclonal anti-β-actin antibody (AC-74, Sigma) were used. Non-reducing SDS-PAGE was performed after preincubation with different concentrations (0, 5, 10, 50 mM) of β-mercaptoethanol (Merck).

GTPase activity measurements

The GTPase activity of mGBP7 was examined with the malachite green assay by determining the release of free inorganic phosphate. The assay was performed as described previously with the given modifications (36, 37). Reactions were carried out in a total volume of 100 µL in 50 mM Tris-HCl, pH 7.5 (at 37 °C) containing 10 mM $MgCl_2$ and 0-5 mM GMP, GDP or GTP. The reaction was initiated by adding 0.68 µM (total amount of protein: 5 µg) or 0.83 µM (total amount of protein: 6.2 µg) of purified mGBP7 protein at 37 °C and stopped after 0 and 20 min by the addition of 25 µL of the reaction mixture into 175 µL of 20 mM ice-cold H_2SO_4. Next, 50 µL of dye solution (0.096% (w/v) malachite green, 1.48% (w/v) ammonium molybdate, and 0.173% (w/v) Tween 20 in 2.36 M H_2SO_4) was added. After 15 min of incubation, the amount of free phosphate was quantified by measuring the absorbance at 595 nm. Obtained data points were fitted using a standard Michaelis-Menten equation (Eq. 1):

$$v = \frac{v_{max}\ [S]}{K_{\mathrm{M}} +\ [S]}$$

Here, v describes the reaction velocity as a function of the substrate concentration [S], v_{max} is the maximum reaction velocity and the Michaelis constant K_{M} denotes the substrate concentration at which the reaction rate is half of v_{max}. It is important to stress that the reaction mechanism of GBPs includes a dimerization step and therefore also dimerization-dependent catalysis. However, the classic Michaelis-Menten equation, which was used in this study, does not account for dimerization-dependent catalysis. In light of the above-mentioned limitations, all kinetic parameters were reported as apparent values to emphasize the point that these equations do not take dimerization processes into account. In addition, the GTPase activity was determined keeping the GTP concentration constant at 2 mM GTP and varying the amount of added protein from 0 to 1 µM (total amount of protein: 0-7.4 µg). Here, the data were fitted using an allosteric sigmoidal (enzyme activity) or a quadratic (specific activity) equation. In this case the reaction was initiated by adding 2 mM GTP and all other steps were performed as described previously. Inhibition of the GTPase activity by γ-phosphate analogues was assayed with 1, 10, and 100 mM stock solutions of BeF_x (Santa Cruz Biotechnology, Inc.) and 1, 10, and 100 mM of $AlCl_3$ complemented with 5, 50, and 500 mM NaF (1, 10, 100 mM AlF_x), respectively. 1, 10, and 100 mM Orthovanadate stock solutions were prepared from Na_3VO_4 (NEB) at pH 10 and boiled for 2 min prior to use (38, 39). To determine the IC_{50} values, the GTPase activity was plotted against the log of inhibitor concentration. The data were analyzed according to the following four parameter logistic equation (Eq. 2):

$$y = \frac{y_{max} - y_{min}}{1 + 10^{((\log IC_{50} - x) \cdot h)}}$$

Here, y represents the GTPase activity value, y_{max} depicts the GTPase activity of the starting plateau and y_{min} depicts the GTPase activity of the final inhibited plateau. x represents the logarithmic concentration of the inhibitor. The Hill slope h describes the steepness of the curve. The half-maximal inhibitory concentration (IC_{50}) is calculated as the value of the inhibitor concentration used at an enzyme activity inhibition of 50%. This value matches the inflection point of the resulting curves.

For data evaluation, an additional reaction with EDTA (final concentration of 20 mM) was performed and the autohydrolysis of GTP was subtracted. A Na_2HPO_4 standard curve was used for the determination of free phosphate concentrations. All experiments were conducted three times. Data were fitted using GraphPad Prism version 5.01 for Windows (GraphPad Software, www.graphpad.com).

Fluorimetry

The fluorescent GTP analogue mant-GTPγS (2‘/3‘-O-(N-Methyl-anthraniloyl)-guanosine-5‘-(γ-thio)-triphosphate (Jena Bioscience) was used to assess the binding affinity of GTP to mGBP7 and to the K51A mGBP7 mutant. The binding of mant-nucleotide to the protein was monitored at 448 nm using a Fluorolog-3 spectrometer (Instruments S.A., HORIBA). The excitation wavelength was set at 355 nm, the slit width at 2 nm, and the temperature was maintained at 25(±1) °C by a circulating water bath. All measurements were done in gel filtration buffer supplemented with 0.5 µM mant-GTPγS. The equilibrium dissociation constant K_D was obtained by fitting the data with a quadratic equation as described previously (7, 40).

MALDI-TOF mass spectrometry

The GTPase activity measurements were carried out in a total volume of 100 µL in 50 mM Tris-HCl, pH 7.5 (at 37 °C) containing 10 mM $MgCl_2$ and 4 mM GTP. The reaction was started by adding 22.5 µM (total amount of protein: 166.2 µg) of purified mGBP7 protein at 37 °C for 30 min. The samples were then spotted with 1 µL of a MALDI matrix solution of α-cyano-4-hydroxy-cinnamic acid (HCCA) in 0,1% trifluoroacetic acid (TFA)/acetonitrile 1:10. MALDI-TOF mass spectrometry was performed on a MALDI-TOF/TOF ultrafleXtreme (Bruker Daltonics). The spectra were recorded in a linear mode within a mass range from *m/z* 200 to *m/z* 3500. The mass spectra were analyzed using flexAnalysis 3.0 (Bruker Daltonics).

Oligomerization and cooperativity analysis

To determine the oligomerization status of mGBP7, a SEC column (Superdex 200 Increase 10/300 GL, GE Healthcare) was equilibrated with gel filtration buffer using a HPLC system (Agilent 1260 HPLC System) connected to a multi-angle light scattering detector (miniDAWN Treos 2, Wyatt technology) and a differential refractive-index detector (Optilab T-rEX differential refractometer, Wyatt technology). 100 µL of purified mGBP7 with a concentration of 3.5 mg/mL (47 µM) or 12 mg/mL (162 µM) were centrifuged for 10 min at 4 °C, preincubated for 5 min with ± 5 mM GTPγS (Jena Bioscience) and loaded onto the equilibrated SEC column at a flow rate of 0.6 ml/min in buffer without added nucleotide. Data collection and processing was performed using the ASTRA7 software (Wyatt Technologies).

BN PAGE was generally performed as described in the Native PAGE Bis-Tris Gel Manual (Thermo Scientific). Prior to BN PAGE analysis, 1.4 µM (total amount of protein: 2 µg) of purified WT or K51A mGBP7 mutant protein were incubated in GTPase buffer for 20 min at 37 °C (or 4 °C, not shown) and supplemented with 2 mM GTPγS or 2 mM GTP in combination with γ-phosphate analogues. Inhibitor concentrations of five times the IC_{50} were used (135 µM Orthovanadate, 1.85 mM AlF_x, and 1.85 mM BeF_x) and the reactions were performed in a total volume of 20 µL. After the incubation, the samples were chilled on ice, supplemented with 5 µL of Native PAGE Sample Buffer and loaded onto a 3-12% Bis-Tris BN PAGE gel. Native PAGE Running Anode Buffer and Native PAGE Dark Blue Cathode Buffer (containing 0.02% Coomassie G-250) were used. Gels were run at 4 °C for 45 min at 150 V and another 45 min at 250 V. Gels were fixed (40% methanol, 10% acetic acid) and de-stained (30% acetic acid) prior to visualization. To estimate molecular masses, denaturated mGBP7 protein was separated electrophoretically. Densitometry analysis was performed using Fiji Software (41) and data were visualized using GraphPad Prism Software version 5.01 for Windows (GraphPad Software, www.graphpad.com). To evaluate the band densities, each lane was measured three times and an appropriate background measurement was substracted. The sum of the protein monomer and dimer densities of each row was set as 100%; the calculated mean values are illustrated in Figure S2A and B.

Homology modeling

Homology modeling was performed using the I-TASSER web server (42-44) to predict the tertiary structure of mGBP7. Only the sequence of mGBP7 (the target) was required as input, while for all other options the default choices were used. First, the top ten sequence alignments to targets of similar folds from the PDB using a meta-threading approach were identified. From this, structure models were produced via Monte Carlo simulations to get thousands of structural conformation variants of the target, which were clustered into five representative models ranked by the cluster-size and their quality based on a confidence score (C-score). The C-score ranges between –5 and +2, with a higher C-score indicating a high structural confidence. Here, the models are also ranked by the C-score. The best I-TASSER model was finally aligned to all structures in the PDB library to identify the ten proteins with the closest structural similarity to the mGBP7 model.

MD simulations of mGBP7 in solution

In order to test the structural stability of the homology models, a 100 ns MD simulation was performed for each of them on the supercomputer JURECA (45). For the preparation, conduct and analysis of the MD simulations, the MD package Gromacs 2016 (46, 47) was applied, using Amber99SB*-ILDNP as protein force field (48, 49) and the TIP3P water model (50). Each system consisted of mGBP7 in the GTP-bound state (GTP and Mg^{2+} ion), water molecules as solvent and 12 Na^{+} ions for neutralization, resulting in a system size of ~200,000 atoms. After simulation-box setup, each system was first relaxed by minimizing the energy to a maximal force of 1000 kJ mol^{-1} nm^{-1} using a steepest descent algorithm and then equilibrated to adapt it to the desired temperature of 310 K and pressure of 1 atm for mimicking the physiological environment. First, a 0.1 ns *NVT* equilibration was performed in which the number of atoms (*N*), the box volume (*V*) and temperature (*T*) were kept constant, followed by a 1 ns *NPT* equilibration to adjust the pressure (*P*). During equilibration, mGBP7 and GTP were restrained with a force constant of 1,000 kJ mol^{-1} nm^{-2}, allowing the water molecules to relax around the solute. Afterwards, the 100 ns MD production runs in the *NPT* ensemble were performed. In order to decrease the computational cost, a triclinic box measuring 10 nm × 10 nm × 19 nm was used and positional restraints were applied on residues of the β-sheets in the G domain so that mGBP7 was not able to rotate within the box. No other restraints were applied during the production runs. The velocity rescaling thermostat (47) was used to regulate the temperature in the *NVT* simulations, while the Nosé-Hoover thermostat (51, 52) and the semi-isotropic Parrinello-Rahman barostat (53) were employed for the *NPT* simulations. The electrostatic interactions were calculated with the particle mesh-Ewald method (54, 55) in connection with periodic boundary conditions. A cutoff of 12 Å was used for the short-range electrostatic and van der Waals interactions. The LINCS algorithm (56) was applied to constrain all bond lengths, allowing for a time step of 2 fs for the integration of the equations of motion. The coordinates and energies of the systems were recorded every 20 ps.

Bioinformatic analyses

To obtain predictions for the secondary structure and transmembrane (TM) propensity based on the mGBP7 sequence, various bioinformatic tools were applied. To identify possible TM regions, three amino acid scales were calculated using the ProtScale web server (57): (i) the Kyte & Doolittle hydrophobicity scale using a window size (ws) of 19 (58), (ii) the transmembrane tendency scale with ws = 9 (59), (iii) the percentage of buried residues scale with ws = 9 (60). For the calculation of these scales, a window size, i.e., the number of residues in the neighborhood of the residue in question that are to be considered needs to be provided. This implies that for the first and last ws/2-1 residues of a given protein sequence these scales are not calculated. The optimal ws depends on the scale to be calculated; the default values as given above were selected in this work. As an additional method to determine TM regions the TMpred server was employed (58). Here, one has to pre-set the possible TM helix length, which was chosed 14-35 residues. TMpred calculates scores for the probability of inside-to-outside and outside-to-inside TM helices. As for mGBP7 the resulting scores were rather similar, the two scores were averaged for each residue. A score value > 0 indicates the presence of a TM helix, and scores > 500 are significant. All bioinformatic tools used in this work required the mGBP7 sequence, for which the sequence with Genbank code DAA05846.1 was used.

MD simulations of the membrane-embedded CT tail

The stability of the membrane-inserted CT tail was tested in an MD simulation. To this end, a system was prepared with residues 590–620 being pre-inserted into a lipid bilayer consisting of 68 POPC molecules. As starting structure the conformation from homology model 3 (Fig. S4) was used, as this is a mainly helical structure in a linear conformation and therefore considered to be good choice for the initial TM helix model. It was inserted in such a way that the amino acids from residue 598 onwards, i.e., where the predicted TM region starts, where in the hydrophobic core of the membrane, whereas residues 590–597 were placed in the head-group region of the upper bilayer leaflet. Charmm36 was used as force field for both the protein (61) and lipids (62), combined with the TIP3P model for water (50) and standard Charmm36 potentials for the 8 K+ and 11 Cl- ions that were added to the system. The resulting system size included 19,770 atoms. For the set-up of the system, its energy minimization and equilibration at a temperature of 310 K and pressure of 1 atm the Charmm-GUI web server (63) was used. The resulting structure, which can be seen in Fig. S6, was subsequently simulated for 250 ns using Gromacs 2016 (47, 48) with the same MD settings used in the simulations of mGBP7 in solution.

Analysis of the MD simulations

To create pictures of the 3D protein structure, PyMol (64) was used. For the calculations, we used Gromacs 2016 (46, 47). To quantify the stability and flexibility of the mGBP7 models during the MD simulations, the root mean square deviations (RMSD) and fluctuations (RMSF) of the C_α atoms of mGBP7 were calculated. The RMSD is the average distance between the atoms of the superimposed homology model and conformations sampled during the MD simulation. For the structural alignment, the last 49 residues were ignored. The RMSF measures the time-averaged fluctuations of the C_α atoms around their average positions. The time-resolved secondary structure of mGBP7 was also determined using the DSSP algorithm (*Define Secondary Structure of Proteins*) (65) to analyze the structural changes of mGBP7 during the MD simulations.

Cell culture and transduction

Primary murine embryonic fibroblasts (MEFs) and Human foreskin fibroblasts (HS27, ATCC) were cultured in Dulbecco's modified Eagle's medium (DMEM, Thermo Scientific) supplemented with 10% (v/v) heat-inactivated low endotoxin fetal bovine serum (FBS, PAN-Biotech), and 0.05 mM β-mercaptoethanol (Thermo Scientific). 293FT cells (Thermo Scientific) were cultivated in DMEM supplemented with 10% FBS, 0.05 mM β-mercaptoethanol and 100 µg/ml penicillin/streptomycin (Merck). All recombinant lentiviruses were produced by transient transfection of 293FT cells as described previously (7). mGBP7$^{-/-}$ MEFs (knockout cell line generated in our laboratory, not shown), were transduced with an appropriate amount of lentivirus and 10 µg/ml polybrene (Merck). After 48 h of incubation, the medium was exchanged by fresh culture medium. Transduced cells were enriched by fluorescence-activated cell sorting (BD FACSAria IIu). Tachyzoites from *T. gondii* strain ME49 (ATCC) were maintained by serial passage using confluent monolayers of HS27 cells as described previously (18).

Infection of MEFs with T. gondii

MEFs were stimulated with 200 U/ml IFNγ (R&D Systems) 16 h prior to infection. For immunofluorescence analysis, MEFs were seeded in 24-well plates (Merck) on 13 mm diameter coverslips (VWR International) and inoculated with freshly harvested *T. gondii* at a ratio of 50 to 1. After 2 hours of incubation, extracellular parasites were removed by washing with PBS (Thermo Scientific).

Immunofluorescence analysis

Cells were fixed with 4% paraformaldehyde (Santa Cruz Biotechnology, Inc.), permeabilized with 0.02% saponin (Merck) in PBS, blocked with 2% goat serum (Agilent Dako) in 0.002% saponin/PBS, and stained as described previously (18). The outer membrane protein SAG1 of *T. gondii* tachyzoites was visualized by anti-SAG1 (Abcam) at a concentration of 1:700 and subsequent incubation with Alexa Fluor 688-conjugated goat anti-rabbit IgG (Sigma) at 1:200. Host cell and pathogen DNA were stained with 1:2500 4,6-diamidino-2-phenylindole (DAPI, Thermo Scientific). The coverslips were fixed on microscope slides using Fluoromount-G (Thermo Scientific). Fluorescence was visualized using an LSM780 confocal microscope with Airyscan detection (Zeiss). Image analysis and processing was performed using ZEN 2012 (blue edition, Zeiss), AutoQuant X3 (MediaCybernetics) and Imaris (Bitplane) software. Quantification data were analyzed by the Student t-test using GraphPad Prism 5.01 (GraphPad Software, www.graphpad.com).

Results

Expression and purification of mGBP7

Previously, we described the biochemical properties of mGBP2 and the GTP hydrolysis deficient mGBP2 mutant K51A (7). In this study, mGBP7 wildtype (WT) protein and a mutated protein (K51A) with an exchange of the lysine residue in the P-loop at position 51 to alanine were analyzed (Fig. 1). Both mGBP7 proteins were expressed in *E. coli* Rosetta^{TM} 2(DE3)pLysS. The highest protein purity was achieved using Ni-NTA batch purification in combination with two consecutive Size Exclusion Chromatography (SEC) steps (Fig. 2A). Purified WT mGBP7 and the K51A mutant were analyzed using Coomassie Brilliant Blue stained SDS gels showing a high purity. WT and K51A mGBP7 were identified by immunoblotting using a polyclonal mGBP7- or a Tetra His-antibody (Fig. 2B-C). Detection of WT mGBP7 with the mGBP7-antibody displayed a slight amount of protein degradation.

GTPase activity of wild type mGBP7 and the K51A mGBP7 mutant

The GTPase activities of WT mGBP7 and the K51A mutant were analyzed using the malachite green phosphate assay by determining the release of free inorganic phosphate. Here, not only GTP but also GDP and GMP were tested as substrates considering that GBPs have the unique feature to hydrolyze GTP to both GDP and GMP (7, 28, 29). Offering GMP to WT mGBP7 and the K51A mutant as a substrate did not result in any measurable phosphate release (Fig. 3A, Tab. 1). Also in the presence of GDP, only a background hydrolysis rate for the purified WT mGBP7 and no phosphate hydrolysis for the K51A mutant were detected (Fig. 3B, Tab.1). In contrast, upon offering GTP a comparable strong GTPase activity with an apparent maximal reaction velocity ($v_{\mathrm{max,\ app}}$) of 265.2 ± 4.7 nmol min^{-1} per mg of protein and an apparent turnover number ($k_{\mathrm{cat,\ app}}$) of 19 min^{-1} for WT mGBP7 were determined. In comparison, the K51A mutant only had a neglectable $v_{\mathrm{max,\ app}}$ of 5.2 ± 4.5 nmol min^{-1} per mg (Fig. 3C, Tab. 1) with a $k_{\mathrm{cat,\ app}}$ of 1 min^{-1} (Fig. 3B, Tab. 1). The obtained hyperbolic curves for the specific activity of WT mGBP7 indicate that there is no cooperativity in relation to GTP binding (Fig. 3C). To corroborate the calculated values for v_{max} and k_{cat}, the GTPase assay was repeated this time varying the amount of added mGBP7 protein and keeping the nucleotide concentration constant at 2 mM GTP (Fig. 3D) (66). Here, plotting the enzyme activity against the mGBP7 concentration a sigmoidal binding curve was obtained (Fig. 3D). This is in agreement with a dimerization-dependent mechanism, in which GTP hydrolysis is promoted by dimerization of the enzyme. In line with this finding, the protein concentration was plotted against the apparent rates yielding an apparent dimerization constant of 0.8 µM for mGBP7. Moreover, the result in Figure 3D indicated that at the used protein concentration of 0.68 µM only about 80% of the protein is active. Therefore, the kinetic parameters of WT mGBP7 were again computed for a concentration of 0.83 µM at which a higher dimer fraction is expected. Here, a higher apparent $v_{\mathrm{max,\ app}}$ of 278.9 ± 9.8 nmol min^{-1}

mg^{-1} and a marginal higher apparent $k_{cat, app}$ of 20 min^{-1} were calculated. This finding demonstrates that the hydrolysis of GTP is concentration-dependent.

In summary, GTPase measurements demonstrate that mGBP7 possesses a high intrinsic GTPase activity and that the K51 is essential for this activity. In addition, the results illustrate that predominantly GTP and not GDP or GMP serve as substrate for the mGBP7 induced hydrolysis reaction.

GTP-binding affinity of wild type mGBP7 and the K51A mGBP7 mutant

To compare the previously studied mGBP2 to mGBP7 analyzed in this study, the GTP-binding affinities of WT mGBP7 and the K51A mutant were examined using fluorescence spectroscopy. The non-hydrolyzable GTP analogue GTPγS labeled with a fluorescent mant group was used as substrate. Interestingly, for WT mGBP7 a K_D of 0.22 µM was determined (Fig. 4). Using the same approach, it was previously demonstrated that WT mGBP2 possesses a high affinity to mant-GTPγS with a K_D of 0.45 µM (7). Thus, it can be concluded that WT mGBP7 has a twofold higher GTP-binding affinity than mGBP2 and that under physiological intracellular conditions mGBP7 is rather expected to exist in the GTP-bound form than nucleotide-free (7). Moreover, whereas for mGBP2 the K51A mutation was described to decrease GTPγS binding affinity drastically (K_D of 44.1 µM), for the K51A mGBP7 mutant virtually no binding in the presence of mant-GTPγS was detected (Fig. 4) (7).

mGBP7 hydrolyzes GTP to GDP and GMP

Previously, we reported for mGBP2 that similar to hGBP1, GMP is the main end product of GTP hydrolysis. Here, the products of mGBP7 specific GTP hydrolysis were determined by Matrix-Assisted Laser Desorption Ionization Time-Of-Flight Mass Spectrometry (MALDI-TOF-MS) which revealed that also for mGBP7, not only GDP but also GMP represents a main product of the GTP-hydrolysis reaction (Fig. 5C). In light of the observation that mGBP7 possesses a high affinity for mant-GTPγS, a control measurement was included to ensure that the purified protein is indeed nucleotide free (Fig. 5A).

mGBP7 forms a transient dimer

The GBP proteins studied to date dimerize upon binding of GTP (7, 67). In previous gel filtration studies, we had demonstrated that mGBP2 elutes as a dimer in the presence of GTPγS (7). Moreover, we had observed that mGBP2 assembles into tetramers in the presence of GDP and AlF_x (7). To address whether mGBP7 is also able to form dimers or even tetramers, the oligomeric state of WT mGBP7 was analyzed via SEC coupled to Multi-Angle Light Scattering (MALS) which allows the determination of the molecular mass of the eluting species independently of their hydrodynamic radius (68). Using this approach, at 3.5 mg/mL protein, an average molecular weight of 74 kDa in the absence of nucleotides and an average molecular weight of 83 kDa after preincubation with 5 mM

GTPγS were determined (Fig. 6A-B). These molar masses are consistent with the monomeric form of the 73.9 kDa His$_6$-mGBP7. At 12 mg/mL protein two molecular species of 93.6 and 142.2 kDa in the absence of nucleotides and two different mGBP7 species of 89.8 and 135.1 kDa in the presence of GTPγS were determined (Fig. 6B-C). However, it has to be noted that the two peaks are eluting too close for a clear separation. Thus, the higher oligomer contains contributions of the lower oligomer and vice versa. This shifts the calculated mass of the dimer toward a lower apparent molecular weight and the monomer toward a higher molecular weight, whereas the shift in the calculated molecular mass of smaller molecules is higher since bigger particles scatter more light. Consequently, when only considering the upper threshold of 148 and 145 kDa for the dimer and the lower threshold of 88 and 83 kDa for the monomer, the calculated values fit quite well to the expected molecular masses of an mGBP7 dimer and monomer, respectively. These data indicate that the mGBP7 dimer formation is rather dependent on protein concentration than affected by the presence of nucleotides. Nevertheless, it has to be considered that the GTPγS nucleotide and the mGBP7 protein possibly get separated in the course of the SEC run and that this is the explanation for the missing shift to more dimer formation. To exclude the possibility that mGBP7 forms a non-physiological disulfide bridge at high protein concentration, SDS-PAGE analyses of the analyzed protein fractions with and without reducing agents were performed (Fig. S3). With and without the reducing agent β-mercaptoethanol, only monomeric mGBP7 was detected indicating that the mGBP7 dimer is not formed due to unspecific disulfide bridge formation.

Thus, it can be postulated that mGBP7 exists in a monomeric and dimeric form and that the addition of GTPγS has no detectable effect on the mGBP7 monomer-to-dimer ratio.

Inhibition of mGBP7 GTPase activity by GTP-transition and ground state analogues

Next, the inhibition of mGBP7-specific GTP hydrolysis by phosphate GTP transition and ground state analogues was analyzed (Fig. 7). To mimic the terminal phosphate group (γ-phosphate) in the transition state, orthovanadate or aluminum fluoride (AlF_x) were added to the reaction mixture. To mimic the γ-phosphate in its ground state, beryllium fluoride (BeF_x) was added to the sample. The GTPase activity is inhibited by binding of orthovanadate, AlF_x, or BeF_x in the position of the γ-phosphate after the first hydrolysis step of the added GTP. To assure that GDP is not the limiting compound for the formation of these GDP-conjugated inhibitor complexes, the measurements were also performed at 4 mM GDP and 2 mM GTP (Fig. S1). In either case, similar concentrations with up to 2 mM of γ-phosphate analogue were required to get a strong (~90%) or nearly complete inhibition of mGBP7 initiated GTP hydrolysis.

Furthermore, the half-maximal inhibitory concentration (IC_{50}) of all three inhibitors was determined (Tab. 2). For orthovanadate, an IC_{50} of 31 μM was calculated, representing the lowest IC_{50} of the examined inhibitors. The IC_{50} for AlF_x was computed to be 405/390 μM, and thus about 13-fold higher than the IC_{50} for orthovanadate. For BeF_x, the IC_{50} was more about in the same range of AlF_x, and with 355/279 μM approx. 10-fold higher than the IC_{50} of Orthovanadate.

Subsequently, it was investigated whether the phosphate analogues could stabilize mGBP7 in its dimeric state. Therefore, the GTPase assay was performed in the presence of GTPγS, orthovanadate, AlF_x, or BeF_x and the samples were analyzed by Blue Native (BN) PAGE (Fig. S2). In all cases, WT proteins were found as both monomers and dimers (Fig. S2A). Also, in the absence of any nucleotides, dimers constituted up to ~8% of the WT mGBP7 proteins. In the presence of the non-hydrolyzable GTP analogues only a very slight increase to ~12% dimers was observed. Subsequently, the K51A mutant was analyzed via BN PAGE (Fig. S2B), and similar monomer-to-dimer ratios were observed.

In summary, these results support the MALS data which demonstrate that the dimerization pattern of mGBP7 is not influenced by the presence of nucleotides.

Homology modeling of mGBP7

To obtain a structure model of mGBP7, homology modeling using Iterative Threading ASSEmbly Refinement (I-TASSER) was employed (42-44). The top ten sequence alignments were found for hGBP1 (Protein Data Bank (PDB) codes 1F5N (69) and 1DG3 (17)) as templates with about 55% sequence identity between mGBP7 and hGBP1. However, in contrast to hGBP1, mGBP7 exhibits no lipid anchor but has 49 additional residues at the C-terminal end (residues 590–638), which will be denoted as C-terminal (CT) tail. Five structure models with C-scores between –1.76 and –0.18 were generated (Fig. S4A), where a larger C-score indicates higher model reliability and a C-score of +2 is the maximum that can be obtained with I-TASSER. The G domain of mGBP7 is very similar to that of hGBP1 as they share a sequence identity of 64%, which was calculated with BLAST (17, 70). As a result, the G domains of the five mGBP7 models differ by less than 0.4 Å in terms of their mutual root mean square deviation (RMSD). Moreover, the GTP-binding sites of mGBP7 and hGBP1 involving loops G1–G4 have similar amino acid compositions (Fig. 8A). It should be noted that N-terminally of the G4 motif in mGBP7 there is a gap compared to hGBP1, shifting D182 of mGBP7 to the position D184 of hGBP1 in the sequence alignment. The structural superposition of the first I-TASSER model of mGBP7 and the hGBP1 crystal structure (PDB code 1F5N (69)) shows that the orientation of the side chains of the key residues R48 and K51 in the P-loop (G1), E99 in switch2, and D182/184 in the G4 motif are slightly different in the two proteins, but overall the structures of the two G domains are very similar to each other (Fig. 8B). For the homology modeling of mGBP7, no GTP was used, therefore, the orientation of the key residues in the GTP-binding site are different between mGBP7 and GNP-bound hGBP1 but they reoriented to the GTP during the MD simulations. The uncertainty of the five I-TASSER models of mGBP7, as evident by the C-scores below zero, stems from the structure prediction for the CT tail, which adopts different helical and/or random coil structures in the five models (Fig. S4). This was confirmed by homology modeling of mGBP7 without the additional 49 C-terminal residues, which resulted in only one model with a high C-score of 1.91, indicating a high reliability of the mGBP7 models for residues 1–589. The best of the five full-length mGBP7 models is shown in Figure 9A. To further elucidate the structural preferences and flexibility of the CT tail, a 100 ns all-atom MD simulation, considering GTP and Mg^{2+} in the active site was performed for each of the five models. These simulations revealed that the CT tail is one of the most flexible parts of mGBP7, which can be deduced from the root mean square fluctuations (RMSF) of the C_α atoms (Fig. 9B and S4C). Another mobile part of mGBP7 is the region where the M and the E regions are connected, resulting from the overall mobility of these two regions with respect to the G domain. Despite this flexibility, the helices in the M and E regions are stable during the MD simulations, which is not the case for the CT tail. The structures at the end point of the MD simulations (Fig. S4B) as well as the analysis of the evolution of the secondary structure (Fig. S5) show that the helices predicted by I-TASSER for some of the last 49 residues are not stable in solution as they started to unfold during the MD simulation. This indicates that the CT tail has a certain propensity for a helical structure, which is, however, not stable in solution but may be stable under different environments, such as a lipid membrane.

To test whether the CT tail may indeed form a transmembrane (TM) helix and might thus act as lipid anchor, which would help in the recruitment of mGBP7 to membranes, various bioinformatic tools, that make such predictions based on the physicochemical properties of the amino acids and their sequence, were employed. First, three amino acid scales using the ProtScale web server (57) were calculated. When interpreted together, these scales allow making predictions about possible TM regions. In particular, the hydrophobicity using the Kyle & Doolittle scale (58), the transmembrane (TM) tendency (59), and the buried-residue probability (60) were calculated for each residue (results not shown). The combination of the three scales led to the identification of three possible TM regions for mGBP7: ^{39}VVVAIVGLY^{47} , ^{114}WIFALAVLL^{121}, both in the G domain, and ^{598}FGDVLISVVPGSGKYFGLGLKIL^{620} in the CT tail. It should be noted that the two possible TM regions identified this way for the G domain are unlikely to be TM helices. Both regions involve only 9 residues, while for a stable TM helix at least 14 residues are required. In addition, residues 39-47 are part of the β-sheet present in the G domain. To support our finding for the CT tail, the TMpred server (58) was invoked. It assigns a score value > 0 to a residue if it is likely to be part of a TM helix. Based on the TMpred results this is the case for the CT tail residues 598-620, i.e., the same residues identified by the combined application of the above mentioned amino acid scales. For some of these residues score values of up to 690 are found, which is above the score threshold of 500 for a significant probability of TM helix formation. Motivated by these findings, in a next step the stability of such a transmembrane CT-tail helix was tested in an MD simulation. To this end, residues 590–620 were pre-inserted into a POPC (phosphatidylcholine) membrane and their dynamics followed for 250 ns. As initial conformation for residues 590–620 the helical conformation from homology model 3 was used, which was placed in the membrane such that residues 590–597 were in head-group region of the upper membrane leaflet, allowing the predicted TM region 598–620 to be located in the hydrophobic membrane core (Fig. S6). During the MD simulation the TM region adopted a tilted conformation (Fig. 9C) as it is longer than the hydrophobic region of a POPC membrane. Another change is that the TM helix is not fully stable as the sequence 598–620 includes two lysine residues, and especially K611 disturbs the TM helix, as it instead prefers to interact with the head-group region of the lower membrane leaflet. Nonetheless, the remaining TM helix is stable, which was not the case during the MD simulations of the corresponding mGBP7 homology model in water, where the CT helix started to unfold within a few nanoseconds (Fig. S5). Thus, based on the current simulations and bioinformatic analysis it is suggested that the CT tail may act as lipid anchor for mGBP7.

The elongated C-terminal tail of mGBP7 is required for its localization in VLS and efficient accumulation at the T. gondii PV

Previously, mGBP2 and several other mGBPs (mGBP1, 3, 6) have been shown to reside in larger complexes in the cytosol of IFNγ-treated cells that we termed vesicle-like structures (VLS) (6, 7, 18, 71). Furthermore, using sophisticated fluorescence microscopy techniques it was shown that mGBPs get depleted of these VLS and relocate quickly to the *T. gondii* PV when the parasite is detected (6).

In an effort, to investigate whether the last 49 C-terminal residues (CT-tail) of mGBP7 are required for the localization of mGBP7 in VLS and/or for the recruitment of mGBP7 to the *T. gondii* PV, we stably transduced mGBP7$^{-/-}$ MEFs with the respective N-terminal GFP fusion constructs. To verify protein expression levels and the integrity of GFP-mGBP7 and GFP-mGBP7$^{\Delta 49}$, Western Blot analyses were performed (Fig. S7A). Confocal microscopy analyses of fixed cells revealed that the truncated mGBP7 (mGBP7$^{\Delta 49}$) does no longer localize in VLS and is evenly distributed within the cytoplasm (Fig. 10A). Moreover, and even more intriguing, *in vitro* analysis of *T. gondii* infected cells demonstrated that in contrast to the WT protein, mGBP7$^{\Delta 49}$ showed significant decreased accumulation effects at the PV of the parasite (Fig. 10B and Fig. S7B).

From these results it can be concluded that the 49 C-terminal residues are essential for the typical mGBP7 localization in VLS and translocation of the protein to the PV of *T. gondii*.

Discussion

In this study, the purification and biochemical characterization of mGBP7 is reported for the first time. mGBP7 is a member of the IFN-inducible GTPase superfamily which has gained attention in the last decades due to its outstanding ability to specifically target intracellular vacuolar pathogens such as *T. gondii* or *C. trachomatis* and to inhibit their replication by leading to the destruction of their vacuolar compartment (6, 72). Previously, we systematically analyzed mGBP2, the closest murine orthologue of hGBP1. For mGBP2, it was demonstrated that different mutations cause individual defects in nucleotide binding, GTPase activity, and oligomerization capability (7). We were particularly interested in examining mGBP7 since this with 638 amino acids largest mGBP family member possesses an elongated C-terminal domain and does not have an isoprenylation motif, in contrast to the previously studied GBPs (GBP1, -2, -5) (7, 13, 15, 23, 25, 73). Furthermore, this study aimed at determining whether mGBP7 shows distinct differences to mGBP2 with respect to GTP affinity, GTP hydrolysis, and domain structure that could help shed light on their individual biological functions in host defense.

The GTP-binding affinity measurement revealed that mGBP7 has a twofold higher affinity for GTP (K_D of 0.22 µM) than mGBP2 and an approx. fivefold higher affinity for GTP than hGBP1 (7, 16, 24, 74). As a result, we propose that under physiological intracellular conditions with about 470 ± 220 µM GTP mGBP7 can efficiently bind and hydrolyze GTP (7, 75). An explanation for this slightly enhanced GTP affinity of mGBP7 compared to hGBP1 and mGBP2 is possibly originating from differences in their GTPase domain and/or minute changes in their conformation. Analysis of the GTP-binding motifs in the G domain reveals that mGBP7 has a ′TVRD′ motif in contrast to hGBP1 and mGBP2 that possess a ′TLRD′ motif (Fig. 8A) (14, 16). This amino acid variation in the G4 motif results in a conservative exchange of aliphatic (L/V) amino acids and could be interesting to analyze by mutational analysis for its effects on GTP-binding affinity. In general, the apparent substrate affinity of mGBP7 for GTP is in the expected range for members of the dynamin superfamily, but is certainly much lower than the GTP-binding affinities of members of the small GTPase families such as Ras or Gα proteins (16). It was previously reported that the K51A mutation drastically impairs the GTP binding affinity for hGBP1 (approx. 50-fold) and mGBP2 (approx. 100-fold) (7, 24). For mGBP7, this effect is even more pronounced, since no binding of the K51A mutant protein to GTPγS was measured, emphasizing the critical role of the K51 residue for nucleotide binding.

First, the GTPase measurements were performed at constant protein concentration to determine the optimal nucleotide concentration, and then the amount of protein was varied to define the protein concentration that is required for 100% protein activity. The GTPase measurements that were finally performed at the optimal mGBP7 concentration and fitted using the Michaelis-Menten equation yielded an apparent $v_{\mathrm{max,\ app}}$ of 278.9 ± 9.8 and an apparent $K_{\mathrm{M,\ app}}$ of 207.0 ± 32.3 µM GTP (Fig. 3C, $\mathrm{WT}_{0.83}$). Furthermore, the obtained sigmoidal binding curve when plotting the enzyme activity in relation to the protein concentration indicated a positive cooperativity of GTP hydrolysis (Fig. 3D). Such positive cooperativity that GTP hydrolysis is promoted enzyme dimerization has previously also been reported for mGBP2 and hGBP1 (7, 17). Another characteristic for GBPs is that they exhibit a high intrinsic GTPase activity. The GBPs usually possess a turnover rate constant k_{cat} of 2-100 min^{-1} and for mGBP2, we could already determine a comparatively high apparent turnover rate of 102 min^{-1} (7). The apparent $k_{\mathrm{cat,\ app}}$ for mGBP7 is 20 min^{-1} (Tab. 1) and therefore fivefold lower than for mGBP2 or hGBP1 (k_{cat} = 95 min^{-1}) but similar to that of hGBP2 with a k_{cat} of 23 min^{-1} (7, 24, 76). A direct comparison of mGBP7, having a twofold higher affinity for GTP, and mGBP2, showing a fivefold greater turnover rate, suggests that the overall catalytic efficiency of mGBP7 and mGBP2 is in about the same range.

According to the GTPase activity measurements, GMP and GDP can only serve as substrates for hydrolysis in negligible amounts. However, the MALDI-TOF-MS results revealed that mGBP7 hydrolyzes GTP to both GDP and GMP proposing a two-step, consecutive hydrolysis mechanism of GTP by mGBP7. For hGBP1, it was shown that GTP hydrolysis to GMP indeed occurs via two consecutive cleavages of single phosphate groups and not by a single cleavage of pyrophosphate (28). We therefore assume that not only hGBP1 (85-90% GMP production) and mGBP2 (74% GMP production) but also mGBP7 releases GMP as reaction product and that the GTP hydrolysis reaction likely involves two consecutive cleavage steps (1, 7, 24). This capability distinguishes mGBP2 and mGBP7 from mGBP5 and hGBP5, which mediate hydrolysis of GTP to GDP only (13, 32). This unique feature of GBPs to hydrolyze GTP to a mixture of GDP and GMP with unequal ratios is quite remarkable and opens up the question of its physiological functions, such as whether GBPs are able to target intracellular pathogens more effectively and/or faster by gaining additional energy from the second hydrolysis step, or whether the production of GMP is beneficial or even necessary for the host response of the target cells. These are questions that will have to be addressed in the future to fully understand the complexity of GBPs in host defense.

The MALS results show that mGBP7 forms a transient dimer and that this dimerization is not influenced by the presence of the non-hydrolyzable GTP analogue GTPγS. Thus, mGBP7 shows a clear difference to the multimerization properties of mGBP2 (7). For WT mGBP2, it was demonstrated in gel filtration studies that it elutes as dimer in the presence of GTPγS but as monomer in the absence of nucleotides (7). These results illustrate that despite the high homology of GBPs, there exist considerable differences in GBP oligomerization behavior that requires further investigation. However, a separated dimer peak was only observed when using very high concentrations of mGBP7 (12 mg/mL). Otherwise, only one broad peak, presumably containing a mixture of monomeric and dimeric species, was observed. This suggests that the dimer formation is transient and that the dimeric state during GTP hydrolysis is only short-lived.

In order to study the oligomerization pattern of mGBP7 in more detail, BN PAGE analyses were performed. First, it was investigated whether mGBP7 GTP hydrolysis could be inhibited by γ-phosphate analogues such as orthovanadate, AlF_x, and BeF_x that trap the GTPase in its ground or transition state of GTP hydrolysis in complex with GDP after the first hydrolysis step. So far, only GDP*AlF_x was analyzed and reported to inhibit hGBP1 and mGBP2 GTP hydrolysis (7, 17). Here, it was shown that besides GDP*AlF_x the GTPase activity of GDP-bound mGBP7 can be inhibited by the two other additionally tested γ-phosphate analogues orthovanadate and BeF_x (Tab. 2). The finding that mGBP7 can be inhibited by AlF_x brings the GBPs closer to the G_α family of proteins that form a stable complex with GDP*AlF_x and the small G proteins that interact with AlF_x in the presence of their respective GTPase-activating proteins (77, 78). Comparable to the MALS result, the BN PAGE analyses that were performed with GTP and excess of γ-phosphate analogues showed almost no effect on the oligomerization pattern of mGBP7 and the mGBP7 K51A mutant. Thus, in contrast to mGBP2, the GTP hydrolysis reaction does not seem to be a prerequisite for the dimerization of mGBP7.

I-TASSER homology modeling revealed that mGBP7 in comparison to hGBP1 possesses an elongated CT tail of 49 residues, which adopts different helical and/or random coil structures and represents one of the most flexible parts of mGBP7. Furthermore, modeling a structure for mGBP7 without the CT tail indicated that the reliability of the proposed five structure models of the truncated mGBP7 is very high. In addition, MD simulations provided evidence that the 49 C-terminal residues are not stable in solution as they started to unfold during the analyzed 100 ns. We consequently propose that the CT tail of mGBP7 has a certain propensity to form a helical structure, which is flexible but unstable in solution (Fig. S4). Moreover, the CT tail alone is predicted to be stable when inserted into a membrane. Thus, this suggested that the CT tail of mGBP7 replaces the role of a Caa*X* motif present in other GBPs (GBP1, -2, and -5) for membrane anchoring.

To test this hypothesis, the subcellular localization of WT mGBP7 and an mGBP7 truncation mutant lacking these last 49 residues (mGBP7$^{\Delta49}$) was investigated in mGBP7$^{-/-}$ cells. WT mGBP7, as previously observed for mGBP2, formed VLS of heterogeneous size in the cytosol (7). In contrast, mGBP7$^{\Delta49}$ showed a more homogeneously distribution and failed to localize to VLS. For mGBP2, this localization to VLS was shown to be dependent on isoprenylation of the Caa*X* box motif (71). In fact, prenylation was reported to be required for the membrane association for all Caa*X* box-containing hGBPs (79). Moreover, the Caa*X* sequences of GBP1, -2 and -5 are conserved which suggests an important biological function and allows speculating if other GBPs might have evolved different structures or modes of membrane interactions to compensate for this binding motif.

In addition, the recruitment potential of mGBP7$^{\Delta49}$ to the outer membrane of the parasite *T. gondii* was assayed since WT mGBP7 and further mGBPs (mGBP1, -2, -3, -6, and -9) efficiently recruit to Toxoplasma parasites (18). Interestingly, there was almost no translocation of mGBP7$^{\Delta49}$ to the PV of *T. gondii* detectable. These results are in line with the MD simulations and propose a nonredundant function of the divergent mGBP7 CT-tail for correct protein localization, membrane anchoring and/or interaction.

Taken together, the GTPase activity, the hydrolyzation products, the structure and the oligomerization pattern of mGBP7 were characterized. Furthermore, the present study demonstrates a so far not described GTP independent mechanism for mGBP7 dimerization and proposes a new mechanism for the interaction of GBPs with intracellular membranes.

Acknowledgements: We would like to thank Julia Mock, Karin Buchholz, Nicole Kuepper, Anne Tersteegen, Jens Lichte, Elisabeth Kravets, Olivia Spitz, and Tobias Beer for experimental assistance, and Ursula R. Sorg for critical reading of the manuscript. Furthermore, we thank Dr. Bogdan Barz for fruitful discussions. Funded by the Deutsche Forschungsgemeinschaft (DFG, German Research Foundation) – project number 267205415 – CRC 1208 to LS, BS, DD, and KP. JL, XW and BS gratefully acknowledge the computing time granted through JARA-HPC (project JICS6A) on the supercomputer JURECA at the Forschungszentrum Juelich.

Conflict of interest: The authors declare that they have no conflicts of interest with the contents of this article.

Author contributions

LL performed all experiments and wrote the paper draft; JL, XW, and BS performed molecular modeling and simulation; NS performed confocal microscopy experiments; MP assisted in MALS experiments; SS and LS assisted in the analysis and interpretation of biochemical and MALS experiments; DD and KP designed and supervised the experiments, assisted in drafting and critical reading. All the authors discussed the results and contributed to the writing of the manuscript.

Figure 1. Domain structure comparison of mGBP7, hGBP1, and mGBP2

(A) All three GBP members contain an N-terminal globular GTPase (G) domain and an extended C-terminal helical domain that can be subdivided in a middle (M) region (α7-11), and a GTPase effector (E) region (α12/13). The G domains encompass the nucleotide-binding motifs G1-G4 (gray, for explanation see introduction). The investigated K51A mutation in the G1 motif of mGBP7 is depicted. Domain structure comparisons of the three GBPs reveal that the mGBP7 E region is approx. 50 amino acids longer than the E region of hGBP1 and mGBP2. Moreover, mGBP7 does not contain a C-terminal Caa*X* motif for isoprenoid modification. (B) Percentage amino acid identity of mGBP7, hGBP1, and mGBP2 (ClustalW alignment).

Figure 2. Purification of wild type mGBP7 and the mGBP7 K51A mutant

(A) SEC profiles of purified WT mGBP7 and the mGBP7 K51A mutant. The mGBP7 proteins containing an N-terminal His_6 tag were expressed in Rosetta^{TM} 2(DE3)pLysS and purified as described under "Experimental Procedures". 5 µg of purified WT mGBP7 (B) and the mGBP7 K51A mutant (C) were resolved on a 4-12% SDS-PAGE and either stained with Coomassie Brilliant Blue (left panel) or detected by Immunoblotting using the polyclonal anti-mGBP7 antibody (middle panel) and the monoclonal anti-Tetra His antibody (right panel). Due to the His_6 tag, mGBP7 has a theoretical mass of 73.9 kDa. mAU, milli-absorbance units.

Figure 3. GTPase activity of purified mGBP7 and the K51A mutant

GTPase activity of WT mGBP7 (blue) and the mGBP7 K51A mutant (red) depending on the GMP (A), GDP (B) or GTP (C) concentration. The GTPase activity was measured in the presence of 0.68 µM (A-C, $WT_{0.68}$ and $K51A_{0.68}$) or 0.83 µM (C, $WT_{0.83}$) protein. In addition, the GTPase activity was measured keeping the GTP concentration constant at 2 mM and varying the mGBP7 concentration (D). Datasets A, B and C were fitted according to the Michaelis-Menten equation (Eq. 1). Dataset D was fitted using an allosteric sigmodal (enzyme activity) or a quadratic (*k*, specific activity) equation, respectively. Results are means ± S.D. from three independent experiments.

Figure 4. Equilibrium binding of mant-GTPγS to mGBP7

WT or K51A mGBP7 was added stepwise to gel filtration buffer containing 0.5 µM mant-GTPγS. The fluorescence was excited at 355 nm and measured at 448 nm. The fluorescence data were analyzed as described under "Experimental Procedures". Results are means ± S.D. from at least three independent experiments. K_D, dissociation constant. CPS, counts per second.

Figure 5. Identification of mGBP7 hydrolysis reaction products

GTPase activity measurements were analyzed by MALDI-TOF-MS. The mass spectrum of a control sample containing mGBP7 but no additional GTP (A), a control sample containing GTP but no protein

(B) and the mass spectrum of a sample containing mGBP7 after the addition of GTP (C) are shown (n=3). Peaks corresponding to mono protonated ions $[M+H]^+$ of GMP, GDP, and GTP are indicated. *m/z*, mass-to-charge ratio.

Figure 6. Concentration-dependent dimerization of mGBP7 assessed by SEC-MALS

Chromatograms of WT mGBP7 showing the differential refractive index (blue) and the calculated molar mass peaks (black). The MALS analyses were performed in the absence of nucleotides (A and C) or after preincubation with 5 mM GTPγS (B and D). At protein concentrations of 3.5 mg/mL (A and B), determined average molar masses were 74 ± 2 kDa (A) and 83 ± 1 kDa (B), respectively. At 12 mg/mL, SEC-MALS elution profiles showed two distinct molecular weight species. Molar mass species in the absence of nucleotides: 142.2 ± 6.9 kDa, 93.6 ± 3.0 kDa. Molar mass species in the presence of GTPγS: 89.8 ± 3.0 kDa, 135.1 ± 6.0 kDa. Including the His_6 tag, the mGBP7 protein has a theoretical mass of 73.9 kDa. SEC, size-exclusion chromatography. MALS, multi-angle light scattering.

Figure 7. Inhibition of mGBP7 by γ-phosphate analogues

GTPase activity of WT mGBP7 in the presence of 0.01, 0.1, 0.5, 1.0 and 2.0 mM orthovanadate (A), AlF_x (B), or BeF_x (C). The GTPase activity was analyzed in the presence of 2 mM GTP and 0.68 µM (5 µg) mGBP7 protein. The data were fitted according to equation 2 (Eq. 2) and the corresponding IC_{50} curves are shown in the insets. Results are means ± S.D. from three independent experiments. IC_{50}, half-maximal inhibitory concentration.

Figure 8. Amino acid sequence and structural alignments of mGBP7 and hGBP1

(A) The sequence alignment between both proteins, calculated by Blast (17, 70) and created with ESPript 3.0 (80), is shown where residues highlighted in red are conserved and residues marked in yellow exhibit similar chemical properties. Furthermore, the four conserved GTP-binding site motifs are displayed: P-Loop (G1) in turquoise, switch1 (G2: T75) in blue, switch2 (G3: DTEG) in magenta, and G4 motif in light orange. The black arrows indicate the key residues for GTP binding and hydrolysis. (B) The G domain of the mGBP7 model 1 (Fig. S4B) is depicted as cartoon. The four GTP-binding loops (cartoon representation) and the key residues (sticks) are highlighted in the corresponding colors as in A. For the comparison of hGBP1 with mGBP7, hGBP1 key residues are shown in gray. The black dashed lines indicate the interactions with GTP (purple sticks).

Figure 9. Homology model for full-length mGBP7 and a model for the membrane-inserted CT tail

(A) The mGBP7 homology model produced by I-TASSER (C-score –0.18) is shown as cartoon, including GTP and Mg^{2+} shown as spheres. mGBP7 consists of three different parts: the G domain (red) with GTP (purple) and Mg^{2+} (orange), the M region (green), the E region (blue) including the C-terminal, 49-residues spanning tail (light blue). The crystal structure of hGBP1 (PDB code 1F5N), which was one of the templates, is overlayed in gray. The RMSD between these two structures is 0.5 Å. (B) The protein flexibility, quantified as the RMSF of the C_α atoms during the MD simulation, is projected onto the mGBP7 model. Rigid residues are displayed in blue and flexible residues in red according to the color scale shown above the protein model. (C) A model for residues 589-620 of the CT tail inserted into a POPC membrane, which was obtained at the end of a 250 ns MD simulation, is shown. Amino acid residues in a helical conformation are colored in blue, coil and turn conformations in gray. The membrane is shown as a yellow transparent surface with the head-group region being indicated by yellow spheres representing the phosphorus atoms.

Figure 10. Subcellular localization of WT mGBP7 and mGBP7$^{\Delta 49}$

Confocal images of N-terminally GFP-tagged mGBP7 proteins in mGBP7$^{-/-}$ MEF cells. Cells were stimulated with IFNγ for 16 h prior to fixation. (A) Intracellular localization of WT mGBP7 (left) and mGBP7$^{\Delta 49}$(right). WT mGBP7 forms distinct subcellular VLS whereas mGBP7$^{\Delta 49}$ shows a mostly homogeneous distribution in the cytoplasm (n = 3). Scale bars, 5 µm. (B) Accumulation of WT mGBP7 and mGBP7$^{\Delta 49}$ at the PV of ME49 *T. gondii* 2 h post infection. WT mGBP7 accumulates at the PV of *T. gondii*. For the truncation mutant mGBP7$^{\Delta 49}$ virtually no accumulation at the PV is detectable. The cell nuclei were stained with DAPI and *T. gondii* was visualized by staining the parasite with the surface marker SAG1 using a mAB to [TP3] (secondary AB: Alexa Fluor 633, cyan). Scale bars, 2 µm.

Supporting Information

Figure S1. Inhibition of mGBP7 by GDP and γ-phosphate analogues

GTPase activity of WT mGBP7 in the presence of 0.01, 0.1, 0.5, 1.0 and 2.0 mM orthovanadate (A) or 0.1, 0.5, 1.0 and 2.0 mM AlF_x/BeF_x (B-C). The GTPase activity was measured in the presence of 2 mM GTP, 4 mM GDP and 2.5 μM (18.5 μg) mGBP7 protein. The data were fitted according to equation 2 (Eq. 2) and the corresponding IC_{50} curves are shown in the insets. Results are means ± S.D. from three independent experiments. IC_{50}, half-maximal inhibitory concentration

Figure S2. Blue Native PAGE of mGBP7 and the K51A mutant

1.4 μM (total amount of protein: 2 μg) of the purified WT mGBP7 or the K51A mutant were incubated in GTPase buffer for 20 min at 37 °C and supplemented with 2 mM GTPγS or GTP in combination with Orthovanadate/AlF_x/BeF_x. WT (A) and K51A mGBP7 (B) samples were analyzed by BN PAGE on a 3-12% Bis-Tris gel. The molecular masses of native markers and the mGBP7 SDS controls are given next to the gel. Densitometry analyses of the bands shown underneath the gels were performed using Fiji Software (41).

Figure S3. SDS-PAGE analyses of WT and K51A mGBP7

5 μg of purified WT mGBP7 (A) or the K51A mutant (B) were incubated with different concentrations of β-mercaptoethanol (0, 5, 10 and 50 mM). After this preincubation step, the samples were mixed with buffer without β-mercaptoethanol and resolved on a 4-12% SDS-PAGE and either stained with Coomassie Brilliant Blue (upper panel) or detected by Immunoblotting using the polyclonal anti-mGBP7 antibody (lower panel). Due to the His_6 tag, mGBP7 has a theoretical mass of 73.9 kDa.

Figure S4. Structural models of mGBP7

(A) The five homology models of mGBP7 determined with I-TASSER and their corresponding C-scores. The protein is shown as cartoon with the G domain shown in red, the M region in green, and the E region in blue. The substrate GTP (spheres) is shown in purple. The C-terminal tail is colored differently for each model. (B) mGBP7 after a 100 ns MD simulation in comparison to the MD starting structure, i.e. the homology model (overlayed in gray) to show the structural changes of the C-terminal tail. (C) The protein flexibility, quantified as the RMSF of the Cα atoms during the MD simulations, is projected onto the mGBP7 models. Rigid residues are displayed in blue and flexible residues in red according to the color scale shown above the protein models.

Figure S5. Secondary structure analysis for the C-terminal tail (residues 590–638) of mGBP7

Time-resolved secondary structure changes for each of the C-terminal residues (y-axis) during the MD simulations are shown. The coil structures (white), β-sheets (red), β-bridges (black), bends (green), turns (yellow), α-helices (blue), 3_{10}-helices (gray), and π-helices (purple) are depicted.

Figure S6. Conformation of residues 589-620 of the CT tail pre-inserted into a POPC bilayer at the start of the MD simulation

Amino acid residues in a helical conformation are shown in blue, coil and turn conformations in gray. The membrane is shown as a yellow transparent surface with the head-group region being indicated by yellow spheres representing the phosphorus atoms.

Figure S7. Western Blot analysis of reconstituted mGBP7$^{-/-}$ cell lines and quantification of PVs targeted by mGBPs

(A) Cell lysates of mGBP7$^{-/-}$ cells reconstituted with GFP-mGBP7 or GFP-mGBP7$^{\Delta 49}$ were resolved on a 4-12% SDS-PAGE and analyzed by immunoblotting using the polyclonal anti-mGBP7 antibody (upper panel) or the monoclonal anti-β-actin antibody (AC-74, Sigma). Due to the GFP tag, mGBP7 has a theoretical mass of 99.8 kDa and mGBP7$^{\Delta 49}$ has a theoretical mass of 94.7 kDa. (B) Quantification of *T. gondii* PVs targeted by mGBPs. At least 100 PVs were counted per experiment. Results are means ± SEM of two independent experiments. 51.0 ± 1.4% of *T. gondii* PVs were targeted by GFP-mGBP7, whereas only 2 ± 1% were targeted by GFP-mGBP$^{\Delta 49}$ (P value 0.0013, P value summary **).

References

1. Vestal DJ, Jeyaratnam JA. The guanylate-binding proteins: emerging insights into the biochemical properties and functions of this family of large interferon-induced guanosine triphosphatase. J Interferon Cytokine Res. 2011;31(1):89-97.
2. Praefcke GJ, McMahon HT. The dynamin superfamily: universal membrane tubulation and fission molecules? Nat Rev Mol Cell Biol. 2004;5(2):133-47.
3. Faelber K, Gao S, Held M, Posor Y, Haucke V, Noe F, et al. Oligomerization of dynamin superfamily proteins in health and disease. Prog Mol Biol Transl Sci. 2013;117:411-43.
4. Haller O, Staeheli P, Schwemmle M, Kochs G. Mx GTPases: dynamin-like antiviral machines of innate immunity. Trends Microbiol. 2015;23(3):154-63.
5. Carter CC, Gorbacheva VY, Vestal DJ. Inhibition of VSV and EMCV replication by the interferon-induced GTPase, mGBP-2: differential requirement for wild-type GTP binding domain. Arch Virol. 2005;150(6):1213-20.
6. Kravets E, Degrandi D, Ma Q, Peulen TO, Klumpers V, Felekyan S, et al. Guanylate binding proteins directly attack Toxoplasma gondii via supramolecular complexes. eLife. 2016;5.
7. Kravets E, Degrandi D, Weidtkamp-Peters S, Ries B, Konermann C, Felekyan S, et al. The GTPase activity of murine guanylate-binding protein 2 (mGBP2) controls the intracellular localization and recruitment to the parasitophorous vacuole of Toxoplasma gondii. J Biol Chem. 2012;287(33):27452-66.
8. Degrandi D, Kravets E, Konermann C, Beuter-Gunia C, Klumpers V, Lahme S, et al. Murine guanylate binding protein 2 (mGBP2) controls Toxoplasma gondii replication. Proc Natl Acad Sci U S A. 2013;110(1):294-9.
9. Lindenberg V, Molleken K, Kravets E, Stallmann S, Hegemann JH, Degrandi D, et al. Broad recruitment of mGBP family members to Chlamydia trachomatis inclusions. PloS one. 2017;12(9):e0185273.
10. Tietzel I, El-Haibi C, Carabeo RA. Human guanylate binding proteins potentiate the anti-chlamydia effects of interferon-gamma. PloS one. 2009;4(8):e6499.
11. Kim BH, Shenoy AR, Kumar P, Das R, Tiwari S, MacMicking JD. A family of IFN-gamma-inducible 65-kD GTPases protects against bacterial infection. Science. 2011;332(6030):717-21.
12. Feeley EM, Pilla-Moffett DM, Zwack EE, Piro AS, Finethy R, Kolb JP, et al. Galectin-3 directs antimicrobial guanylate binding proteins to vacuoles furnished with bacterial secretion systems. Proceedings of the National Academy of Sciences of the United States of America. 2017;114(9):E1698-E706.
13. Shenoy AR, Wellington DA, Kumar P, Kassa H, Booth CJ, Cresswell P, et al. GBP5 promotes NLRP3 inflammasome assembly and immunity in mammals. Science. 2012;336(6080):481-5.
14. Kresse A, Konermann C, Degrandi D, Beuter-Gunia C, Wuerthner J, Pfeffer K, et al. Analyses of murine GBP homology clusters based on in silico, in vitro and in vivo studies. BMC Genomics. 2008;9:158.
15. Cheng YS, Patterson CE, Staeheli P. Interferon-induced guanylate-binding proteins lack an N(T)KXD consensus motif and bind GMP in addition to GDP and GTP. Mol Cell Biol. 1991;11(9):4717-25.
16. Praefcke GJ, Geyer M, Schwemmle M, Robert Kalbitzer H, Herrmann C. Nucleotide-binding characteristics of human guanylate-binding protein 1 (hGBP1) and identification of the third GTP-binding motif. J Mol Biol. 1999;292(2):321-32.
17. Prakash B, Praefcke GJ, Renault L, Wittinghofer A, Herrmann C. Structure of human guanylate-binding protein 1 representing a unique class of GTP-binding proteins. Nature. 2000;403(6769):567-71.
18. Degrandi D, Konermann C, Beuter-Gunia C, Kresse A, Wurthner J, Kurig S, et al. Extensive characterization of IFN-induced GTPases mGBP1 to mGBP10 involved in host defense. J Immunol. 2007;179(11):7729-40.
19. Olszewski MA, Gray J, Vestal DJ. In silico genomic analysis of the human and murine guanylate-binding protein (GBP) gene clusters. J Interferon Cytokine Res. 2006;26(5):328-52.

20. Vopel T, Hengstenberg CS, Peulen TO, Ajaj Y, Seidel CA, Herrmann C, et al. Triphosphate induced dimerization of human guanylate binding protein 1 involves association of the C-terminal helices: a joint double electron-electron resonance and FRET study. Biochemistry. 2014;53(28):4590-600.

21. Nantais DE, Schwemmle M, Stickney JT, Vestal DJ, Buss JE. Prenylation of an interferon-gamma-induced GTP-binding protein: the human guanylate binding protein, huGBP1. J Leukoc Biol. 1996;60(3):423-31.

22. Vopel T, Syguda A, Britzen-Laurent N, Kunzelmann S, Ludemann MB, Dovengerds C, et al. Mechanism of GTPase-activity-induced self-assembly of human guanylate binding protein 1. J Mol Biol. 2010;400(1):63-70.

23. Ince S, Kutsch M, Shydlovskyi S, Herrmann C. The human guanylate-binding proteins hGBP-1 and hGBP-5 cycle between monomers and dimers only. FEBS J. 2017;284(14):2284-301.

24. Praefcke GJ, Kloep S, Benscheid U, Lilie H, Prakash B, Herrmann C. Identification of residues in the human guanylate-binding protein 1 critical for nucleotide binding and cooperative GTP hydrolysis. J Mol Biol. 2004;344(1):257-69.

25. Wehner M, Kunzelmann S, Herrmann C. The guanine cap of human guanylate-binding protein 1 is responsible for dimerization and self-activation of GTP hydrolysis. FEBS J. 2012;279(2):203-10.

26. Kochs G, Haller O. Chapter 226 - Mx Proteins: High Molecular Weight GTPases with Antiviral Activity. In: Bradshaw RA, Dennis EA, editors. Handbook of Cell Signaling (Second Edition). San Diego: Academic Press; 2010. p. 1855-64.

27. Tripathi R, Glaves R, Marx D. The GTPase hGBP1 converts GTP to GMP in two steps via proton shuttle mechanisms. Chem Sci. 2017;8(1):371-80.

28. Schwemmle M, Staeheli P. The interferon-induced 67-kDa guanylate-binding protein (hGBP1) is a GTPase that converts GTP to GMP. J Biol Chem. 1994;269(15):11299-305.

29. Ghosh A, Praefcke GJ, Renault L, Wittinghofer A, Herrmann C. How guanylate-binding proteins achieve assembly-stimulated processive cleavage of GTP to GMP. Nature. 2006;440(7080):101-4.

30. Abdullah N, Balakumari M, Sau AK. Dimerization and its role in GMP formation by human guanylate binding proteins. Biophysical journal. 2010;99(7):2235-44.

31. Fres JM, Muller S, Praefcke GJ. Purification of the CaaX-modified, dynamin-related large GTPase hGBP1 by coexpression with farnesyltransferase. J Lipid Res. 2010;51(8):2454-9.

32. Wehner M, Herrmann C. Biochemical properties of the human guanylate binding protein 5 and a tumor-specific truncated splice variant. FEBS J. 2010;277(7):1597-605.

33. Cheng YS, Colonno RJ, Yin FH. Interferon induction of fibroblast proteins with guanylate binding activity. J Biol Chem. 1983;258(12):7746-50.

34. Kim BH, Shenoy AR, Kumar P, Bradfield CJ, MacMicking JD. IFN-inducible GTPases in host cell defense. Cell Host Microbe. 2012;12(4):432-44.

35. pWPXL was a gift from Didier Trono (Addgene plasmid # 12257 ; http://n2t.net/addgene:12257 ; RRID:Addgene_12257).

36. Baykov AA, Evtushenko OA, Avaeva SM. A malachite green procedure for orthophosphate determination and its use in alkaline phosphatase-based enzyme immunoassay. Analytical Biochemistry. 1988;171(2):266-70.

37. Reimann S, Poschmann G, Kanonenberg K, Stuhler K, Smits SH, Schmitt L. Interdomain regulation of the ATPase activity of the ABC transporter haemolysin B from Escherichia coli. Biochem J. 2016;473(16):2471-83.

38. Gordon JA. [41] Use of vanadate as protein-phosphotyrosine phosphatase inhibitor. Methods in Enzymology. 201: Academic Press; 1991. p. 477-82.

39. Kluth M, Stindt J, Dröge C, Linnemann D, Kubitz R, Schmitt L. A mutation within the extended X loop abolished substrate-induced ATPase activity of the human liver ATP-binding cassette (ABC) transporter MDR3. The Journal of biological chemistry. 2015;290(8):4896-907.

40. Herrmann C, Nassar N. Ras and its effectors. Prog Biophys Mol Biol. 1996;66(1):1-41.

41. Schindelin J, Arganda-Carreras I, Frise E, Kaynig V, Longair M, Pietzsch T, et al. Fiji: an open-source platform for biological-image analysis. Nat Methods. 2012;9(7):676-82.
42. Yang J, Yan R, Roy A, Xu D, Poisson J, Zhang Y. The I-TASSER Suite: protein structure and function prediction. Nat Methods. 2015;12(1):7-8.
43. Roy A, Kucukural A, Zhang Y. I-TASSER: a unified platform for automated protein structure and function prediction. Nat Protoc. 2010;5(4):725-38.
44. Zhang Y. I-TASSER server for protein 3D structure prediction. Bmc Bioinformatics. 2008;9.
45. Mitoma H, Hanabuchi S, Kim T, Bao M, Zhang Z, Sugimoto N, et al. The DHX33 RNA helicase senses cytosolic RNA and activates the NLRP3 inflammasome. Immunity. 2013;39(1):123-35.
46. Abraham MJ, Murtola T, Schulz R, Páll S, Smith JC, Hess B, et al. GROMACS: High performance molecular simulations through multi-level parallelism from laptops to supercomputers. SoftwareX. 2015;1-2:19-25.
47. Abraham MJ, van der Spoel, D., Lindahl, E., Hess, B., the GROMACS development team GROMACS User Manual version 2016.4 2018 [www.gromacs.org].
48. Best RB, Hummer G. Optimized molecular dynamics force fields applied to the helix-coil transition of polypeptides. J Phys Chem B. 2009;113(26):9004-15.
49. Aliev AE, Kulke M, Khaneja HS, Chudasama V, Sheppard TD, Lanigan RM. Motional timescale predictions by molecular dynamics simulations: case study using proline and hydroxyproline sidechain dynamics. Proteins. 2014;82(2):195-215.
50. Jorgensen WL, Chandrasekhar J, Madura JD, Impey RW, Klein ML. Comparison of Simple Potential Functions for Simulating Liquid Water. J Chem Phys. 1983;79(2):926-35.
51. Hoover WG. Canonical dynamics: Equilibrium phase-space distributions. Phys Rev A Gen Phys. 1985;31(3):1695-7.
52. Nose S. A Molecular-Dynamics Method for Simulations in the Canonical Ensemble. Mol Phys. 1984;52(2):255-68.
53. Parrinello M, Rahman A. Polymorphic Transitions in Single-Crystals - a New Molecular-Dynamics Method. J Appl Phys. 1981;52(12):7182-90.
54. Darden T, York D, Pedersen L. Particle Mesh Ewald - an N.Log(N) Method for Ewald Sums in Large Systems. J Chem Phys. 1993;98(12):10089-92.
55. Essmann U, Perera L, Berkowitz ML, Darden T, Lee H, Pedersen LG. A Smooth Particle Mesh Ewald Method. J Chem Phys. 1995;103(19):8577-93.
56. Hess B, Bekker H, Berendsen HJC, Fraaije JGEM. LINCS: A linear constraint solver for molecular simulations. J Comput Chem. 1997;18(12):1463-72.
57. Gasteiger E, Hoogland C, Gattiker A, Duvaud Se, Wilkins MR, Appel RD, et al. Protein Identification and Analysis Tools on the ExPASy Server. In: Walker JM, editor. The Proteomics Protocols Handbook. Totowa, NJ: Humana Press; 2005. p. 571-607.
58. Kyte J, Doolittle RF. A simple method for displaying the hydropathic character of a protein. J Mol Biol. 1982;157(1):105-32.
59. Zhao G, London E. An amino acid "transmembrane tendency" scale that approaches the theoretical limit to accuracy for prediction of transmembrane helices: relationship to biological hydrophobicity. Protein science : a publication of the Protein Society. 2006;15(8):1987-2001.
60. Janin J. Surface and inside volumes in globular proteins. Nature. 1979;277(5696):491-2.
61. Huang J, MacKerell AD, Jr. CHARMM36 all-atom additive protein force field: validation based on comparison to NMR data. J Comput Chem. 2013;34(25):2135-45.
62. Pastor RW, Mackerell AD, Jr. Development of the CHARMM Force Field for Lipids. The journal of physical chemistry letters. 2011;2(13):1526-32.
63. Jo S, Kim T, Iyer VG, Im W. CHARMM-GUI: a web-based graphical user interface for CHARMM. J Comput Chem. 2008;29(11):1859-65.
64. L DeLano W. The PyMOL Molecular Graphics System (2002) DeLano Scientific, Palo Alto, CA, USA. http://www.pymol.org2002.
65. Kabsch W, Sander C. Dictionary of Protein Secondary Structure - Pattern-Recognition of Hydrogen-Bonded and Geometrical Features. Biopolymers. 1983;22(12):2577-637.

66. Zaitseva J, Jenewein S, Wiedenmann A, Benabdelhak H, Holland IB, Schmitt L. Functional characterization and ATP-induced dimerization of the isolated ABC-domain of the haemolysin B transporter. Biochemistry. 2005;44(28):9680-90.

67. Praefcke GJK. Regulation of innate immune functions by guanylate-binding proteins. Int J Med Microbiol. 2017.

68. Wyatt PJ. Submicrometer Particle Sizing by Multiangle Light Scattering following Fractionation. J Colloid Interface Sci. 1998;197(1):9-20.

69. Prakash B, Renault L, Praefcke GJ, Herrmann C, Wittinghofer A. Triphosphate structure of guanylate-binding protein 1 and implications for nucleotide binding and GTPase mechanism. EMBO J. 2000;19(17):4555-64.

70. Altschul SF, Wootton JC, Gertz EM, Agarwala R, Morgulis A, Schaffer AA, et al. Protein database searches using compositionally adjusted substitution matrices. FEBS J. 2005;272(20):5101-9.

71. Vestal DJ, Gorbacheva VY, Sen GC. Different subcellular localizations for the related interferon-induced GTPases, MuGBP-1 and MuGBP-2: implications for different functions? J Interferon Cytokine Res. 2000;20(11):991-1000.

72. Meunier E, Broz P. Interferon-inducible GTPases in cell autonomous and innate immunity. Cellular microbiology. 2016;18(2):168-80.

73. Modiano N, Lu YE, Cresswell P. Golgi targeting of human guanylate-binding protein-1 requires nucleotide binding, isoprenylation, and an IFN-gamma-inducible cofactor. Proc Natl Acad Sci U S A. 2005;102(24):8680-5.

74. Kunzelmann S, Praefcke GJ, Herrmann C. Nucleotide binding and self-stimulated GTPase activity of human guanylate-binding protein 1 (hGBP1). Methods Enzymol. 2005;404:512-27.

75. Traut TW. Physiological concentrations of purines and pyrimidines. Mol Cell Biochem. 1994;140(1):1-22.

76. Neun R, Richter MF, Staeheli P, Schwemmle M. GTPase properties of the interferon-induced human guanylate-binding protein 2. FEBS Lett. 1996;390(1):69-72.

77. Bigay J, Deterre P, Pfister C, Chabre M. Fluoroaluminates activate transducin-GDP by mimicking the gamma-phosphate of GTP in its binding site. FEBS Lett. 1985;191(2):181-5.

78. Ahmadian MR, Mittal R, Hall A, Wittinghofer A. Aluminum fluoride associates with the small guanine nucleotide binding proteins. FEBS Lett. 1997;408(3):315-8.

79. Britzen-Laurent N, Bauer M, Berton V, Fischer N, Syguda A, Reipschlager S, et al. Intracellular trafficking of guanylate-binding proteins is regulated by heterodimerization in a hierarchical manner. PLoS One. 2010;5(12):e14246.

80. Robert X, Gouet P. Deciphering key features in protein structures with the new ENDscript server. Nucleic Acids Res. 2014;42(Web Server issue):W320-4.

Table 1

Kinetic parameters of mGBP7 GTPase activity in the presence of different nucleotides. Results are means ± S.D. from three independent experiments. $v_{\mathrm{max,\ app}}$, apparent maximal reaction velocity. $K_{\mathrm{m,\ app}}$, apparent Michaelis-Menten constant. $k_{\mathrm{cat,\ app}}$, apparent turnover number. ND, not detected.

	GTP			GDP			GMP		
	$v_{\mathrm{max,\ app}}$	$K_{\mathrm{m,\ app}}$	$k_{\mathrm{cat,\ app}}$	$v_{\mathrm{max,\ app}}$	$K_{\mathrm{m,\ app}}$	$k_{\mathrm{cat,\ app}}$	v_{max}	$K_{\mathrm{m,\ app}}$	$k_{\mathrm{cat,\ app}}$
	nmol min⁻¹ mg⁻¹	*µM GTP*	*min⁻¹*	*nmol min⁻¹ mg⁻¹*	*µM GDP*	*min⁻¹*	*nmol min⁻¹ mg⁻¹*	*µM GMP*	*min⁻¹*
$\mathrm{WT}_{0.83}$	278.9 ± 9.8[a]	207.0 ± 32.3[a]	20[a]	-	-	-	-	-	-
$\mathrm{WT}_{0.68}$	265.2 ± 4.7[b]	323.4 ± 21.7[b]	19[b]	ND	ND	ND	ND	ND	ND
WT	-	-	20[c]	-	-	-	-	-	-
K51A	5.2 ± 4.5[b]	ND	1[b]	ND	ND	ND	ND	ND	ND

[a] The GTPase activity was measured in the presence of 0.83 µM (total amount of protein: 6.2 µg) mGBP7 protein ($\mathrm{WT}_{0.83}$, Fig. 3 C).

[b] The GTPase activity was measured in the presence of 0.68 µM (total amount of protein: 5 µg) mGBP7 protein ($\mathrm{WT}_{0.68}$, Fig. 3 A-C).

[c] The GTPase activity was measured in the presence of 2 mM GTP (WT, Fig. 3 D).

Table 2

IC_{50} values of mGBP7 GTPase activity inhibited by γ-phosphate analogues. Results are means ± S.D. from three independent experiments. IC_{50}, half-maximal inhibitory concentration.

γ-phosphate analogue	
Orthovanadate	31 ± 2[a]
	31 ± 6[b]
AlF_x	405 ± 61[a]
	390 ± 48[b]
BeF_x	355 ± 53[a]
	279 ± 71[b]

[a] The GTPase activity was measured in the presence of 2 mM GTP and 0.68 µM (total amount of protein: 5 µg) mGBP7 protein.

[b] The GTPase activity was measured in the presence of 2 mM GTP, 4 mM GDP and 2.5 µM (total amount of protein: 18.5 µg) mGBP7 protein.

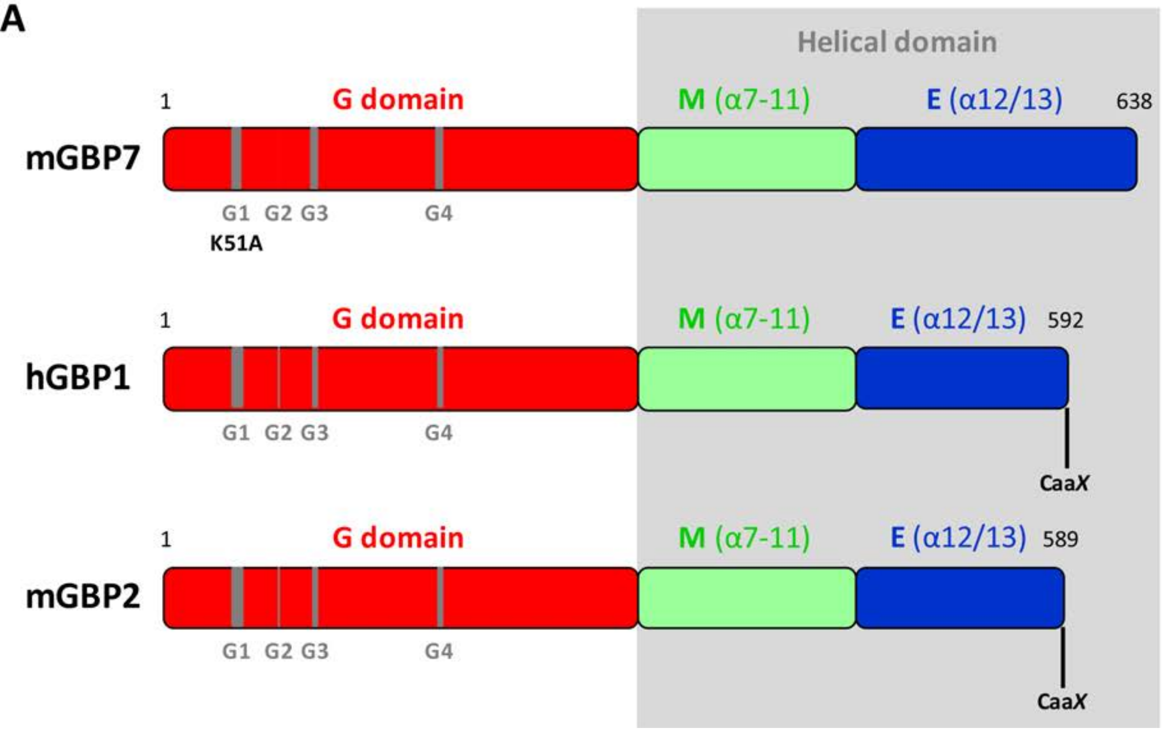

B

	mGBP7	hGBP1	mGBP2
mGBP7		50.6%	48.1%
hGBP1	50.6%		68.0%
mGBP2	48.1%	68.0%	

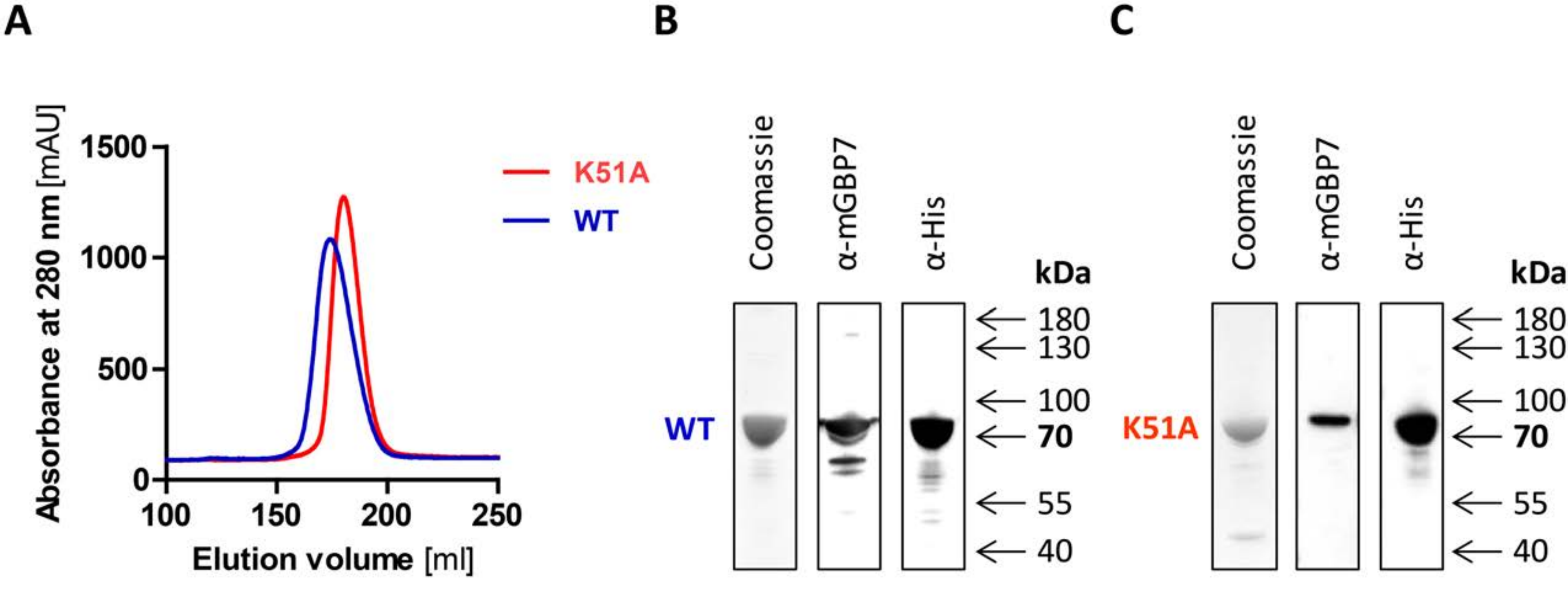
A
B
C
Absorbance at 280 nm [mAU]
1500
1000
500
0
100
150
200
250
Elution volume [ml]
K51A
WT
Coomassie
α-mGBP7
α-His
kDa
180
130
100
70
55
40
WT
Coomassie
α-mGBP7
α-His
kDa
180
130
100
70
55
40
K51A

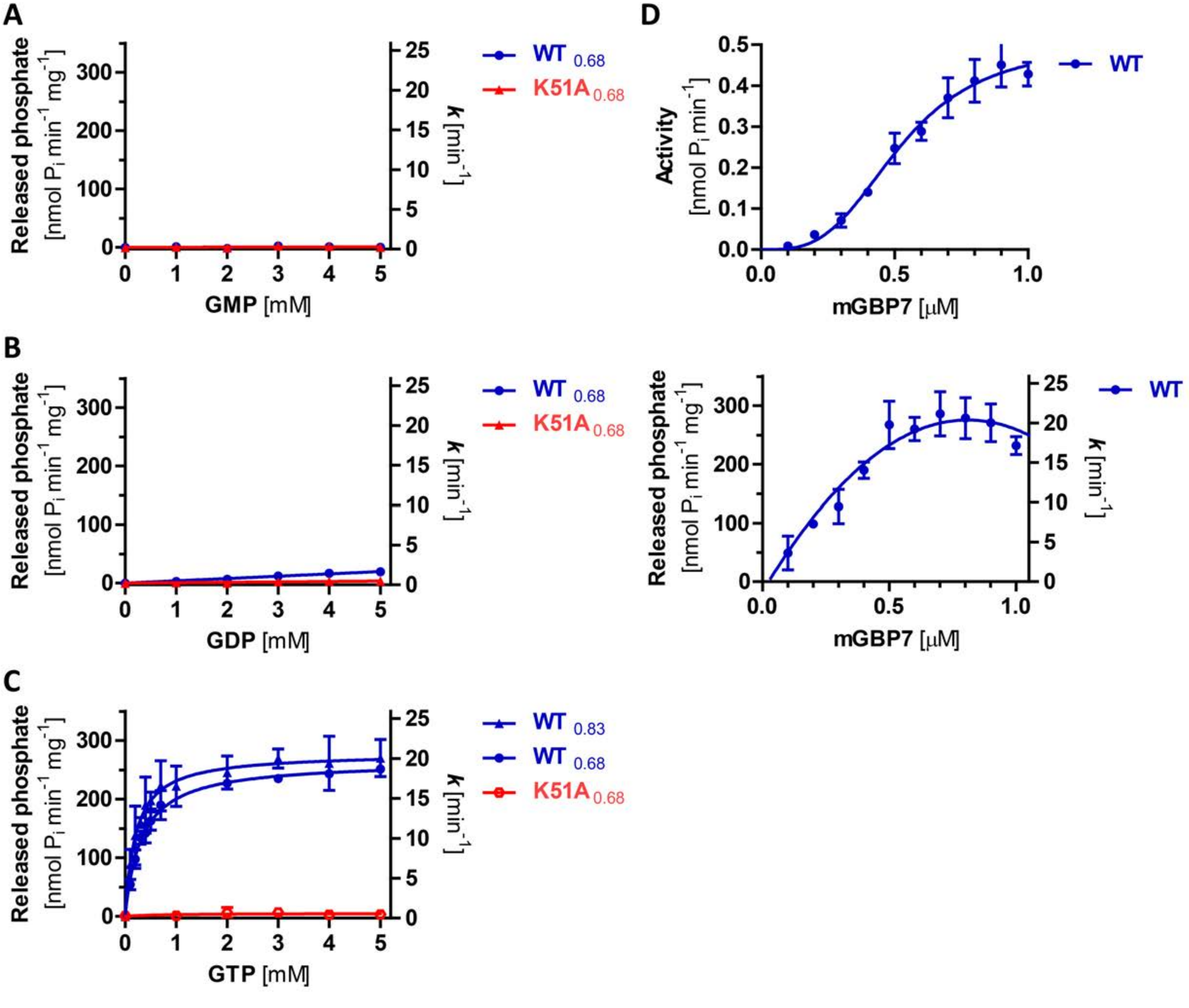
A
Released phosphate [nmol P_i min^-1 mg^-1]
0
100
200
300
k [min^-1]
0
5
10
15
20
25
0
1
2
3
4
5
GMP [mM]
WT 0.68
K51A 0.68
B
Released phosphate [nmol P_i min^-1 mg^-1]
0
100
200
300
k [min^-1]
0
5
10
15
20
25
0
1
2
3
4
5
GDP [mM]
WT 0.68
K51A 0.68
C
Released phosphate [nmol P_i min^-1 mg^-1]
0
100
200
300
k [min^-1]
0
5
10
15
20
25
0
1
2
3
4
5
GTP [mM]
WT 0.83
WT 0.68
K51A 0.68
D
Activity [nmol P_i min^-1]
0.0
0.1
0.2
0.3
0.4
0.5
0.0
0.5
1.0
mGBP7 [µM]
WT
Released phosphate [nmol P_i min^-1 mg^-1]
0
100
200
300
k [min^-1]
0
5
10
15
20
25
0.0
0.5
1.0
mGBP7 [µM]
WT

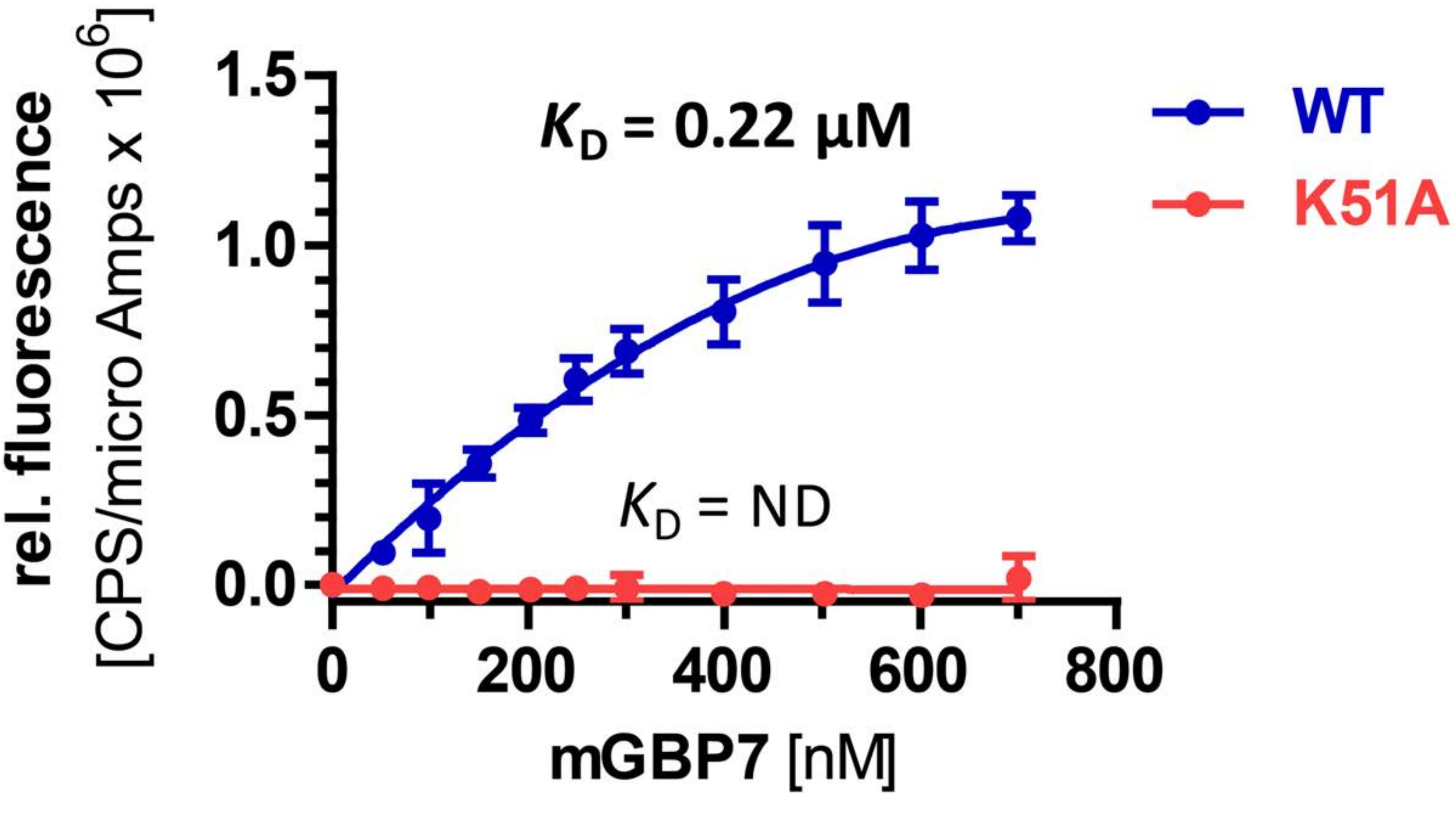
rel. fluorescence
[CPS/micro Amps x 10^6]
1.5
1.0
0.5
0.0
0
200
400
600
800
mGBP7 [nM]
K_D = 0.22 µM
K_D = ND
WT
K51A

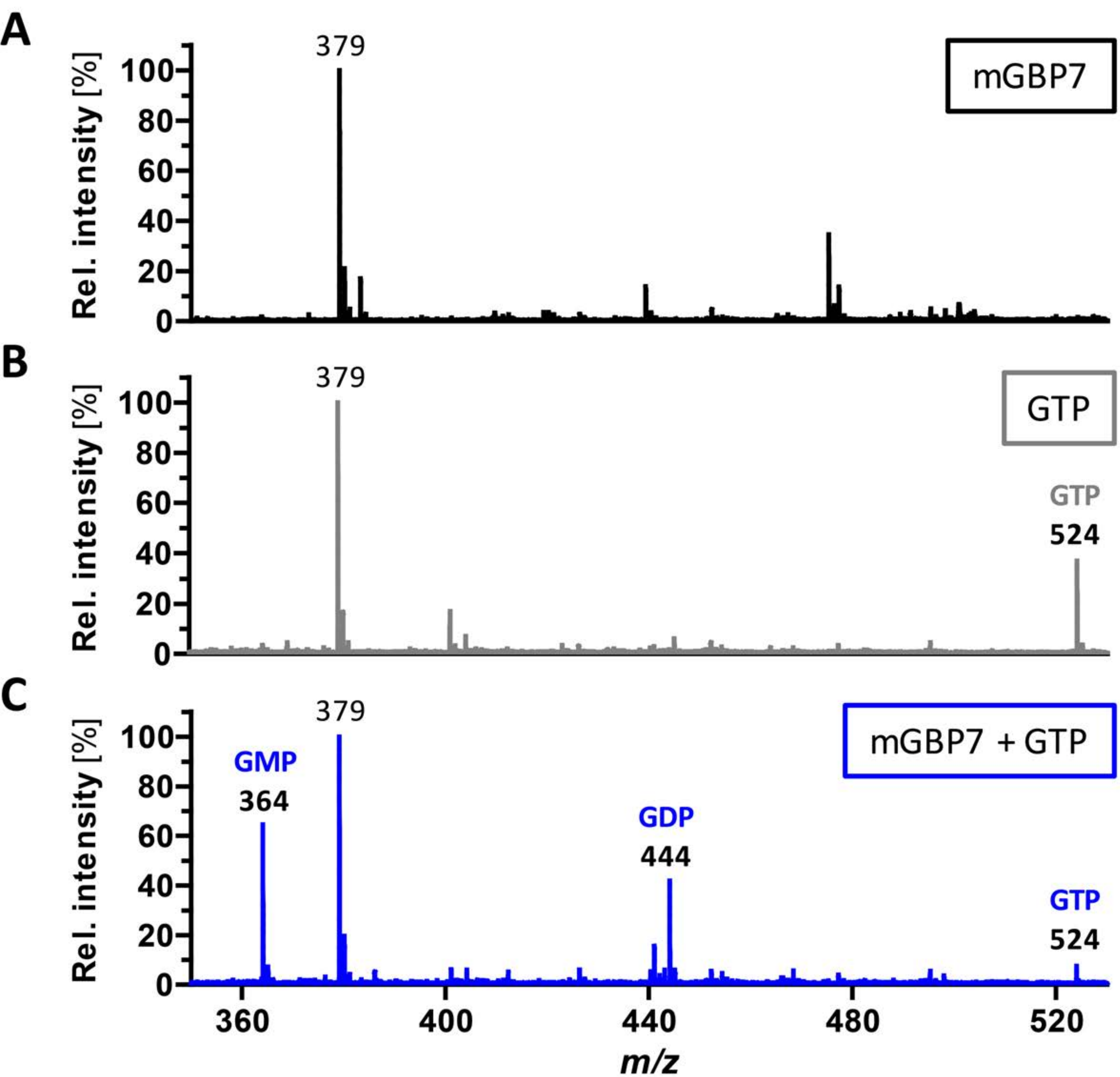
A
379
mGBP7
Rel. intensity [%]
100
80
60
40
20
0
B
379
GTP
GTP
524
Rel. intensity [%]
100
80
60
40
20
0
C
379
mGBP7 + GTP
GMP
364
GDP
444
GTP
524
Rel. intensity [%]
100
80
60
40
20
0
360
400
440
480
520
m/z

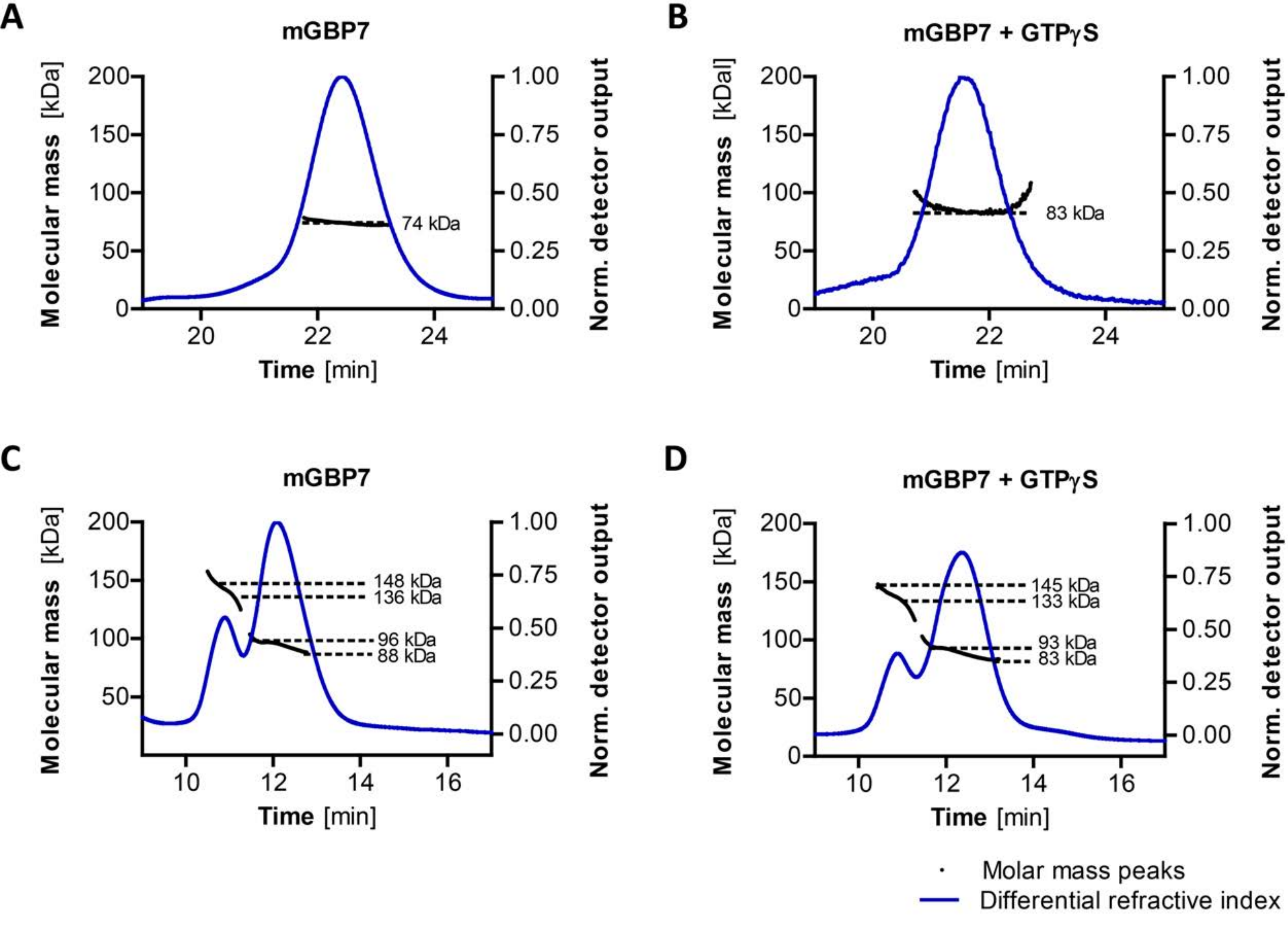
A
mGBP7
Molecular mass [kDa]
200
150
100
50
0
Norm. detector output
1.00
0.75
0.50
0.25
0.00
74 kDa
20
22
24
Time [min]
B
mGBP7 + GTPγS
Molecular mass [kDa]
200
150
100
50
0
Norm. detector output
1.00
0.75
0.50
0.25
0.00
83 kDa
20
22
24
Time [min]
C
mGBP7
Molecular mass [kDa]
200
150
100
50
Norm. detector output
1.00
0.75
0.50
0.25
0.00
148 kDa
136 kDa
96 kDa
88 kDa
10
12
14
16
Time [min]
D
mGBP7 + GTPγS
Molecular mass [kDa]
200
150
100
50
0
Norm. detector output
1.00
0.75
0.50
0.25
0.00
145 kDa
133 kDa
93 kDa
83 kDa
10
12
14
16
Time [min]
Molar mass peaks
Differential refractive index

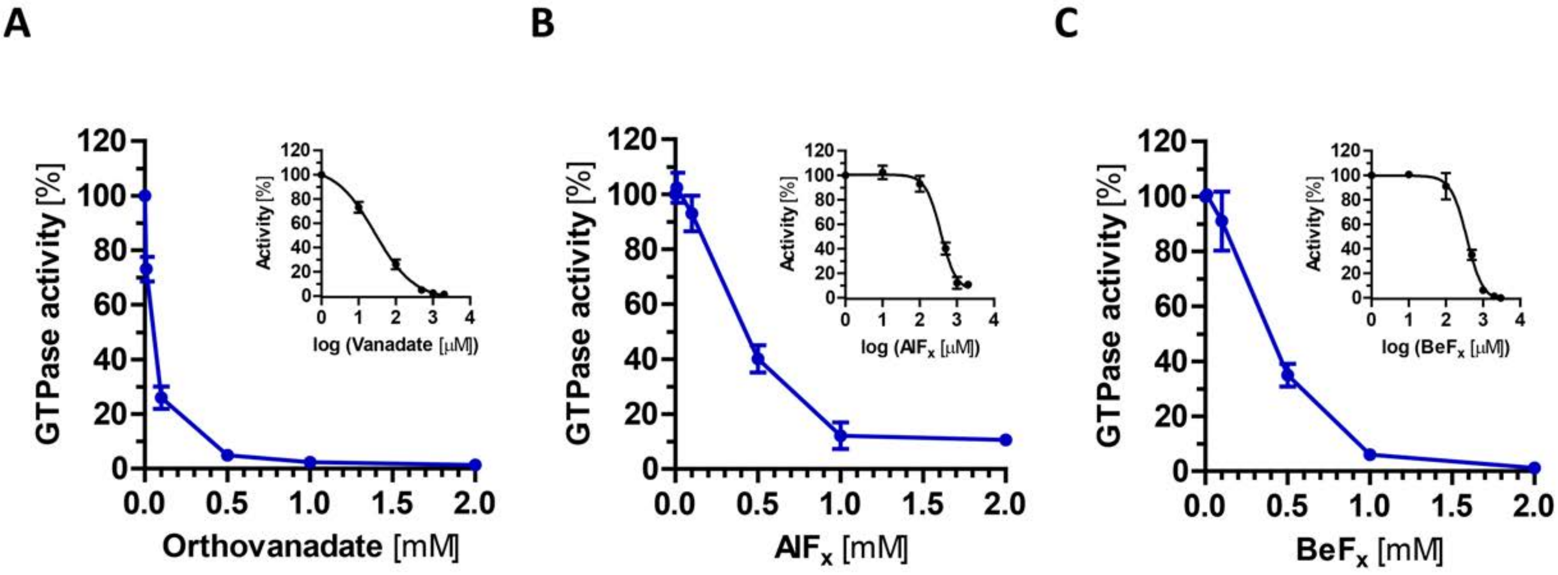
A
GTPase activity [%]
120
100
80
60
40
20
0
0.0
0.5
1.0
1.5
2.0
Orthovanadate [mM]
Activity [%]
log (Vanadate [μM])
B
GTPase activity [%]
AlF$_x$ [mM]
Activity [%]
log (AlF$_x$ [μM])
C
GTPase activity [%]
BeF$_x$ [mM]
Activity [%]
log (BeF$_x$ [μM])
0
1
2
3
4

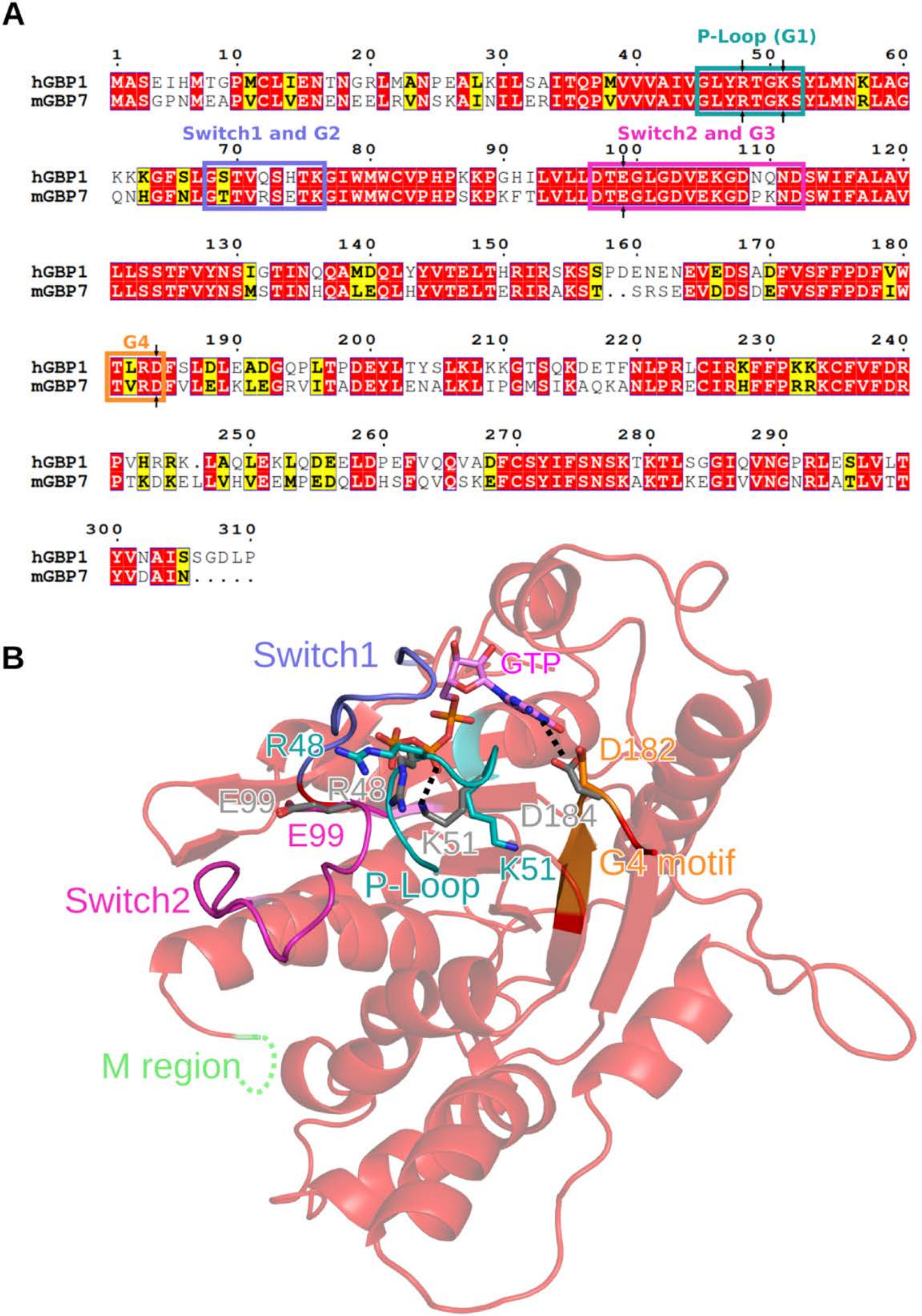
A
P-Loop (G1)
Switch1 and G2
Switch2 and G3
G4
1 10 20 30 40 50 60
hGBP1 MASEIHMTGPMCLIENTNGRLMANPEALKILSAITQPMVVVAIVGLYRTGKSYLMNKLAG
mGBP7 MASGPNMEAPVCLVENENEELRVNSKAINILERITQPVVVVAIVGLYRTGKSYLMNRLAG
70 80 90 100 110 120
hGBP1 KKKGFSLGSTVQSHTKGIWMWCVPHPKKPGHILVLLDTEGLGDVEKGDNQNDSWIFALAV
mGBP7 QNHGFNLGTTVRSETKGIWMWCVPHPSKPKFTLVLLDTEGLGDVEKGDPKNDSWIFALAV
130 140 150 160 170 180
hGBP1 LLSSTFVYNSIGTINQQAMDQLYYVTELTHRIRSKSSPDENENEVEDSADFVSFFPDFVW
mGBP7 LLSSTFVYNSMSTINHQALEQLHYVTELTERIRAKST..SRSEEVDDSDEFVSFFPDFIW
190 200 210 220 230 240
hGBP1 TLRDFSLDLEADGQPLTPDEYLTYSLKLKKGTSQKDETFNLPRLCIRKFFPKKKCFVFDR
mGBP7 TVRDFVLELKLEGRVITADEYLENALKLIPGMSIKAQKANLPRECIRHFFPRRKCFVFDR
250 260 270 280 290
hGBP1 PVHRRK.LAQLEKLQDEELDPEFVQQVADFCSYIFSNSKTKTLSGGIQVNGPRLESLVLT
mGBP7 PTKDKELLVHVEEMPEDQLDHSFQVQSKEFCSYIFSNSKAKTLKEGIVVNGNRLATLVTT
300 310
hGBP1 YVNAISSGDLP
mGBP7 YVDAIN.....
B
Switch1
GTP
R48
D182
R48
E99
E99
D184
K51
K51
G4 motif
P-Loop
Switch2
M region

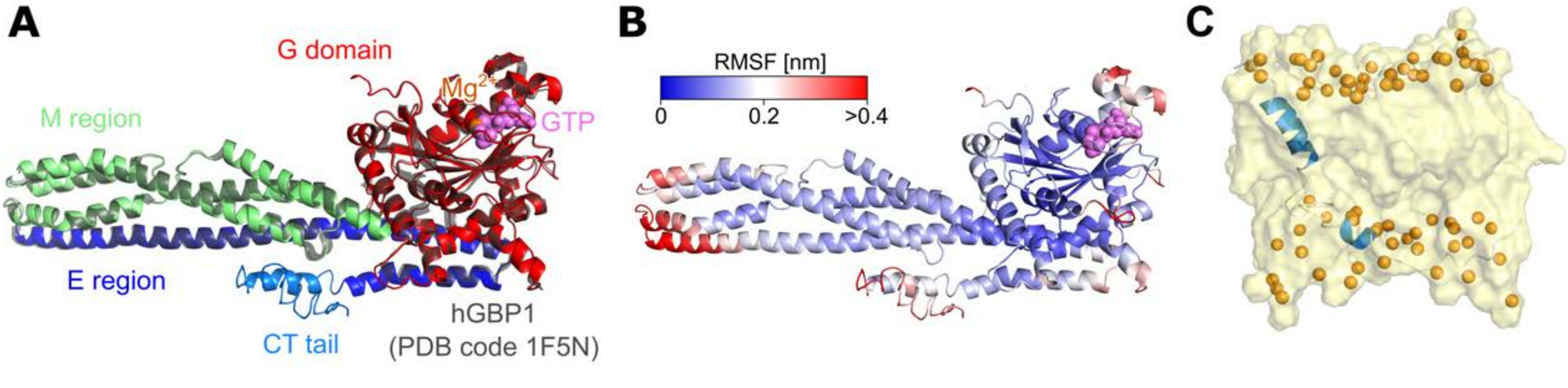
A
G domain
Mg2+
GTP
M region
E region
CT tail
hGBP1
(PDB code 1F5N)
B
RMSF [nm]
0
0.2
>0.4
C

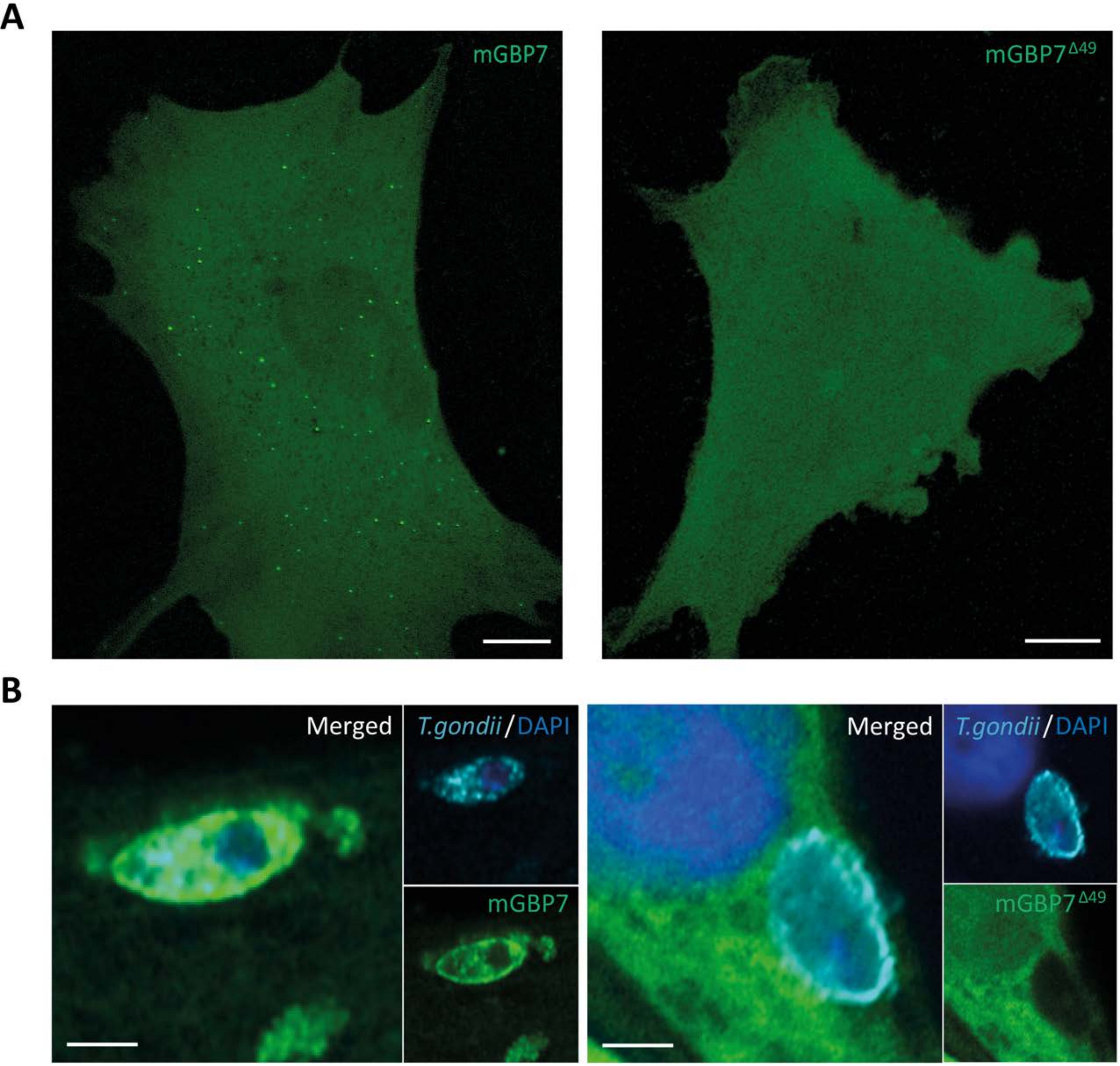
A
mGBP7
mGBP7Δ49
B
Merged
T.gondii / DAPI
mGBP7
Merged
T.gondii / DAPI
mGBP7Δ49

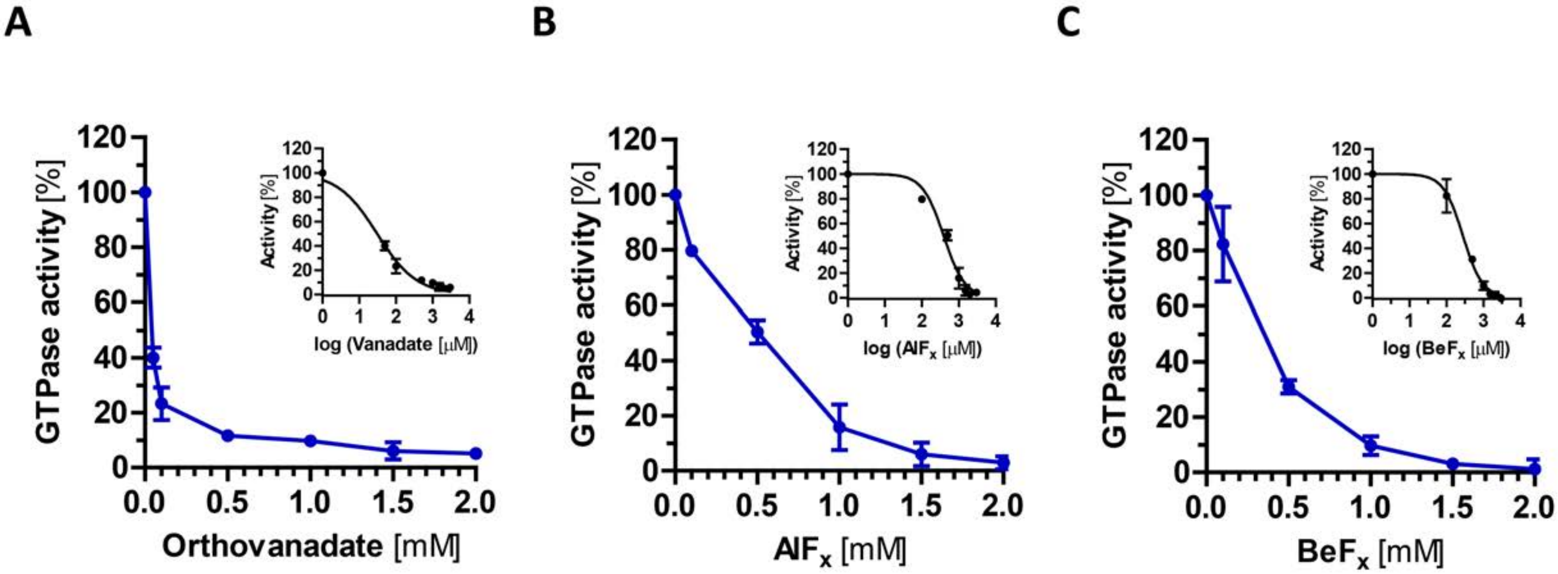
A
GTPase activity [%]
120
100
80
60
40
20
0
0.0
0.5
1.0
1.5
2.0
Orthovanadate [mM]
Activity [%]
log (Vanadate [μM])
0
1
2
3
4
B
GTPase activity [%]
AlF$_x$ [mM]
Activity [%]
log (AlF$_x$ [μM])
C
GTPase activity [%]
BeF$_x$ [mM]
Activity [%]
log (BeF$_x$ [μM])

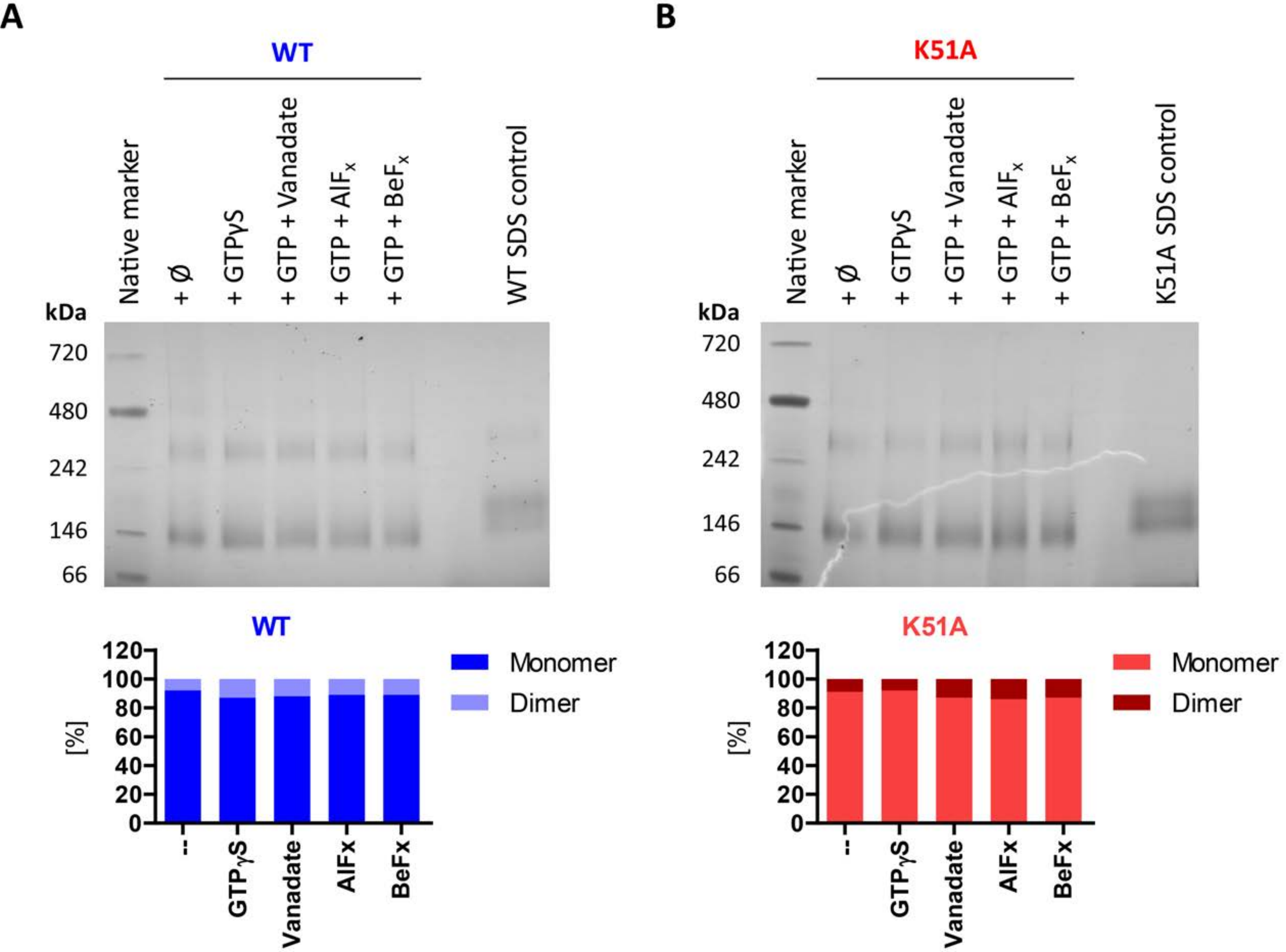
A
WT
Native marker
+ Ø
+ GTPγS
+ GTP + Vanadate
+ GTP + AlF$_x$
+ GTP + BeF$_x$
WT SDS control
kDa
720
480
242
146
66
WT
120
100
80
60
40
20
0
[%]
Monomer
Dimer
--
GTPγS
Vanadate
AlFx
BeFx
B
K51A
Native marker
+ Ø
+ GTPγS
+ GTP + Vanadate
+ GTP + AlF$_x$
+ GTP + BeF$_x$
K51A SDS control
kDa
720
480
242
146
66
K51A
120
100
80
60
40
20
0
[%]
Monomer
Dimer
--
GTPγS
Vanadate
AlFx
BeFx

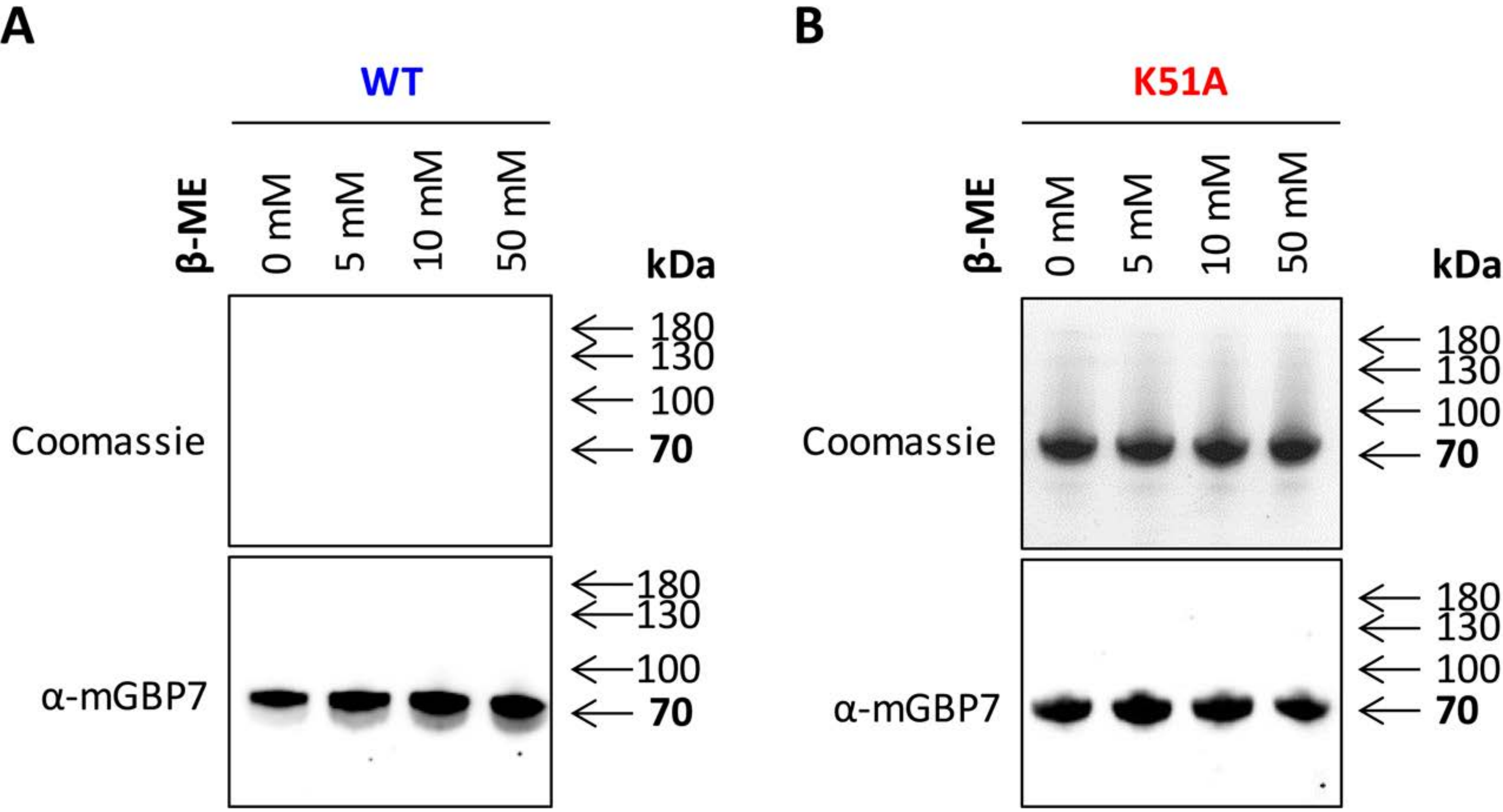
A
WT
β-ME
0 mM
5 mM
10 mM
50 mM
kDa
180
130
100
70
Coomassie
180
130
100
70
α-mGBP7
B
K51A
β-ME
0 mM
5 mM
10 mM
50 mM
kDa
180
130
100
70
Coomassie
180
130
100
70
α-mGBP7

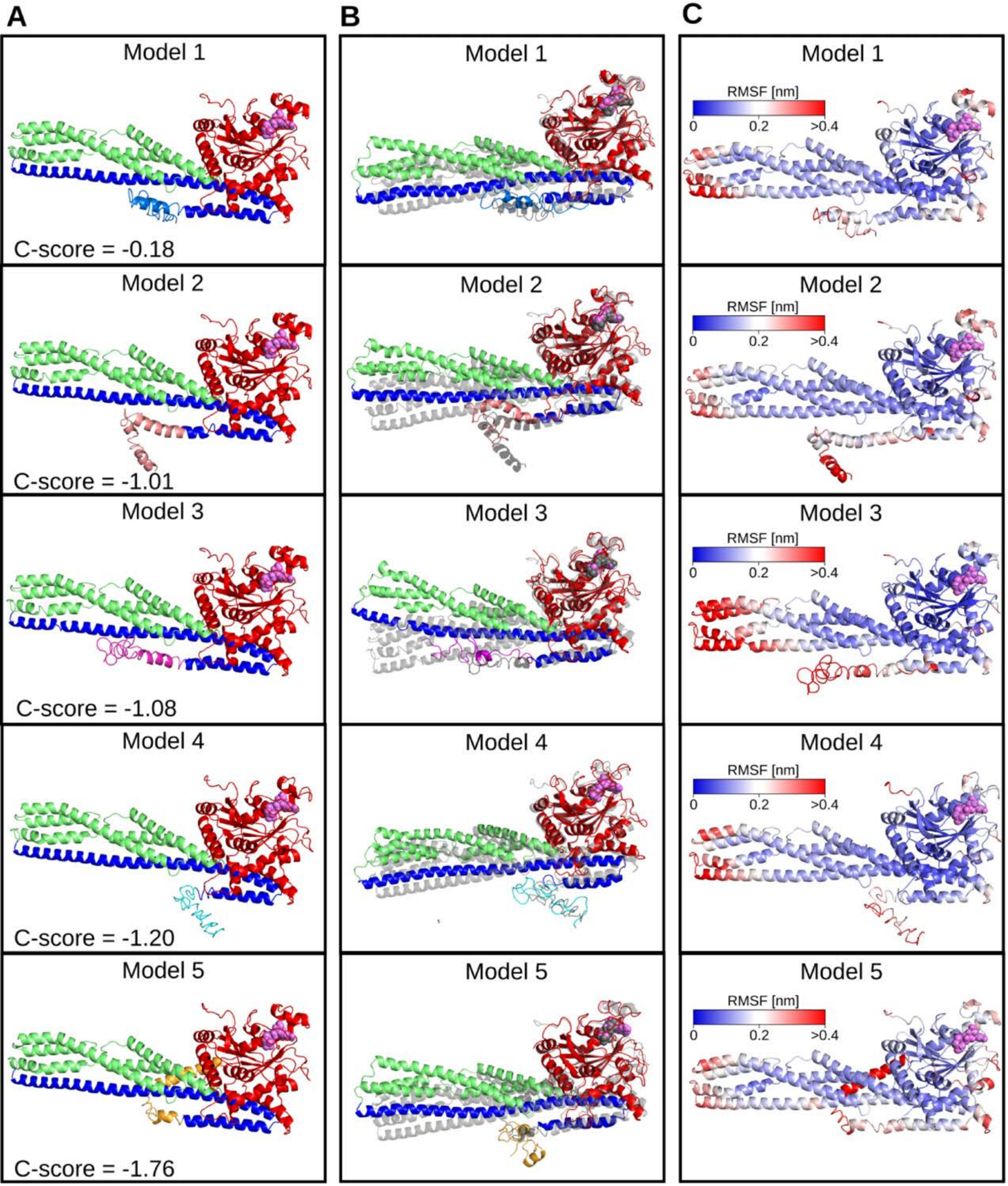
A
Model 1
C-score = -0.18
Model 2
C-score = -1.01
Model 3
C-score = -1.08
Model 4
C-score = -1.20
Model 5
C-score = -1.76
B
Model 1
Model 2
Model 3
Model 4
Model 5
C
Model 1
RMSF [nm]
0
0.2
>0.4
Model 2
RMSF [nm]
0
0.2
>0.4
Model 3
RMSF [nm]
0
0.2
>0.4
Model 4
RMSF [nm]
0
0.2
>0.4
Model 5
RMSF [nm]
0
0.2
>0.4

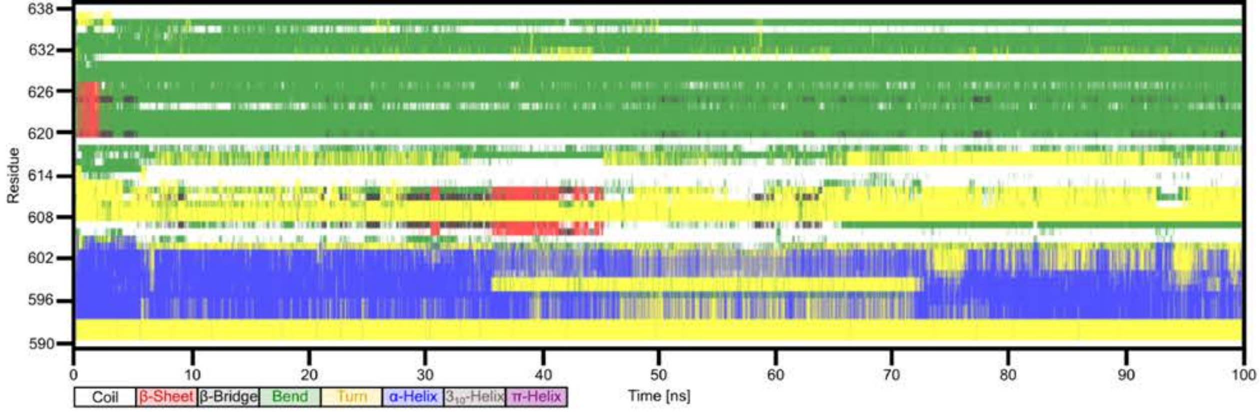
638
632
626
620
614
608
602
596
590
Residue
0
10
20
30
40
50
60
70
80
90
100
Time [ns]
Coil
β-Sheet
β-Bridge
Bend
Turn
α-Helix
3_{10}-Helix
π-Helix

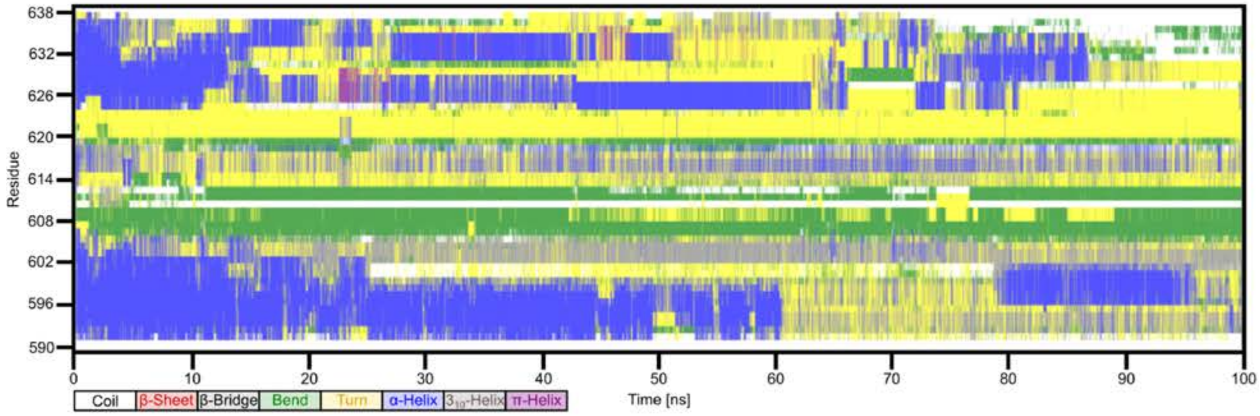
638
632
626
620
614
608
602
596
590
Residue
0
10
20
30
40
50
60
70
80
90
100
Time [ns]
Coil
β-Sheet
β-Bridge
Bend
Turn
α-Helix
3_{10}-Helix
π-Helix

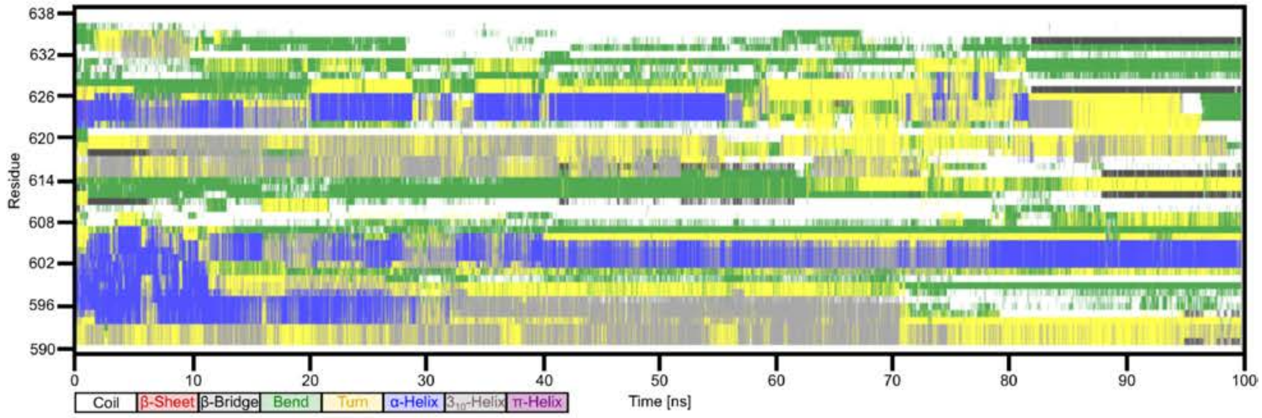
638
632
626
620
614
608
602
596
590
Residue
0
10
20
30
40
50
60
70
80
90
100
Time [ns]
Coil
β-Sheet
β-Bridge
Bend
Turn
α-Helix
3_{10}-Helix
π-Helix

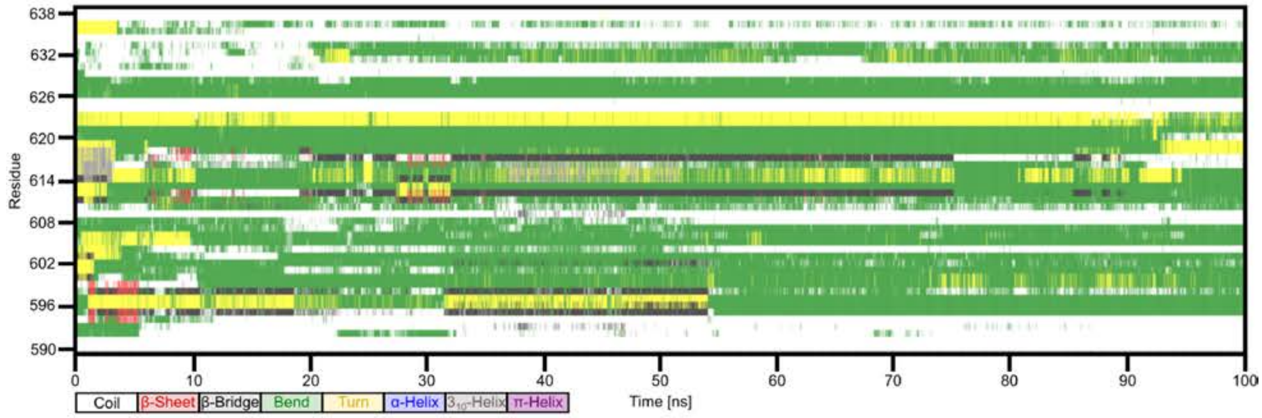
638
632
626
620
614
608
602
596
590
Residue
0
10
20
30
40
50
60
70
80
90
100
Time [ns]
Coil
β-Sheet
β-Bridge
Bend
Turn
α-Helix
3_{10}-Helix
π-Helix

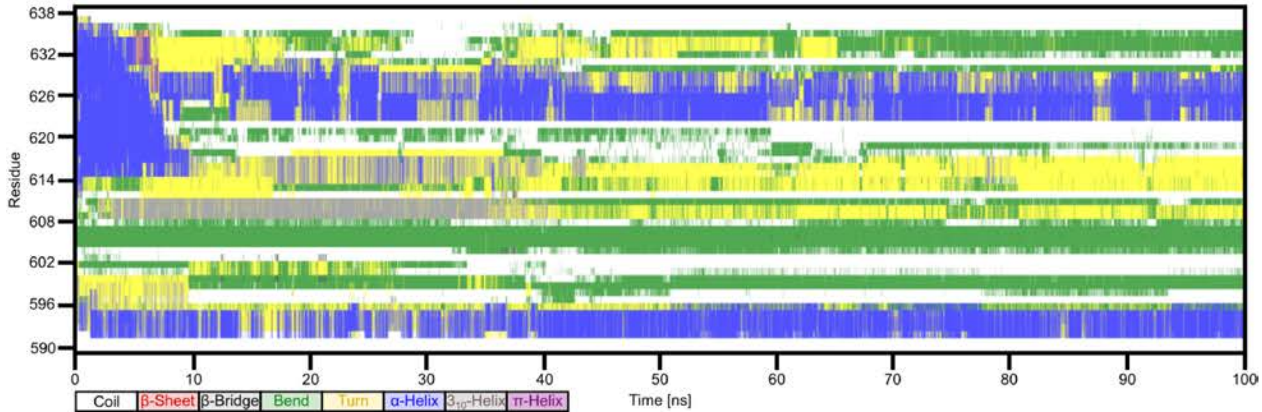
638
632
626
620
614
608
602
596
590
Residue
0
10
20
30
40
50
60
70
80
90
100
Time [ns]
Coil
β-Sheet
β-Bridge
Bend
Turn
α-Helix
3_{10}-Helix
π-Helix

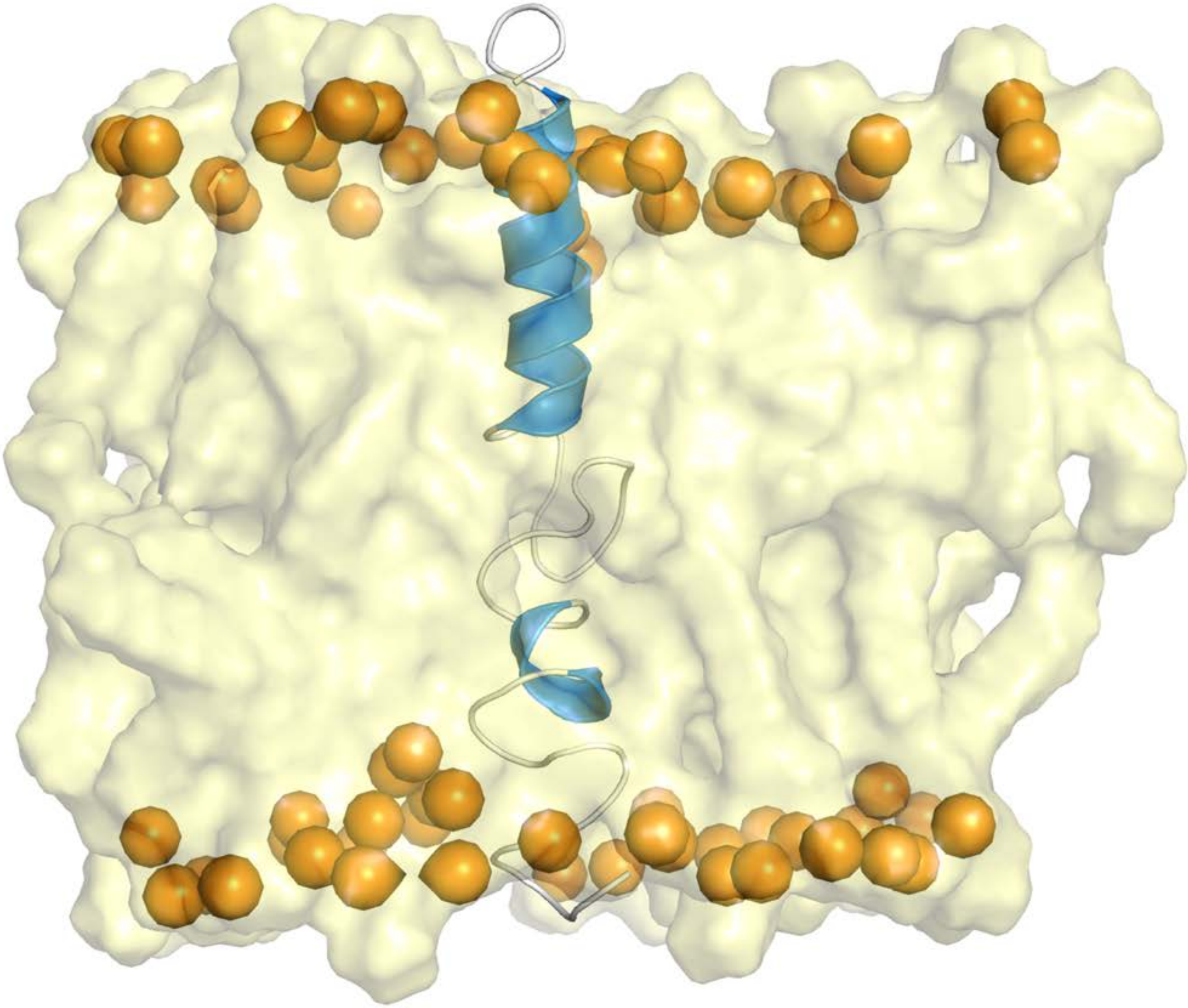

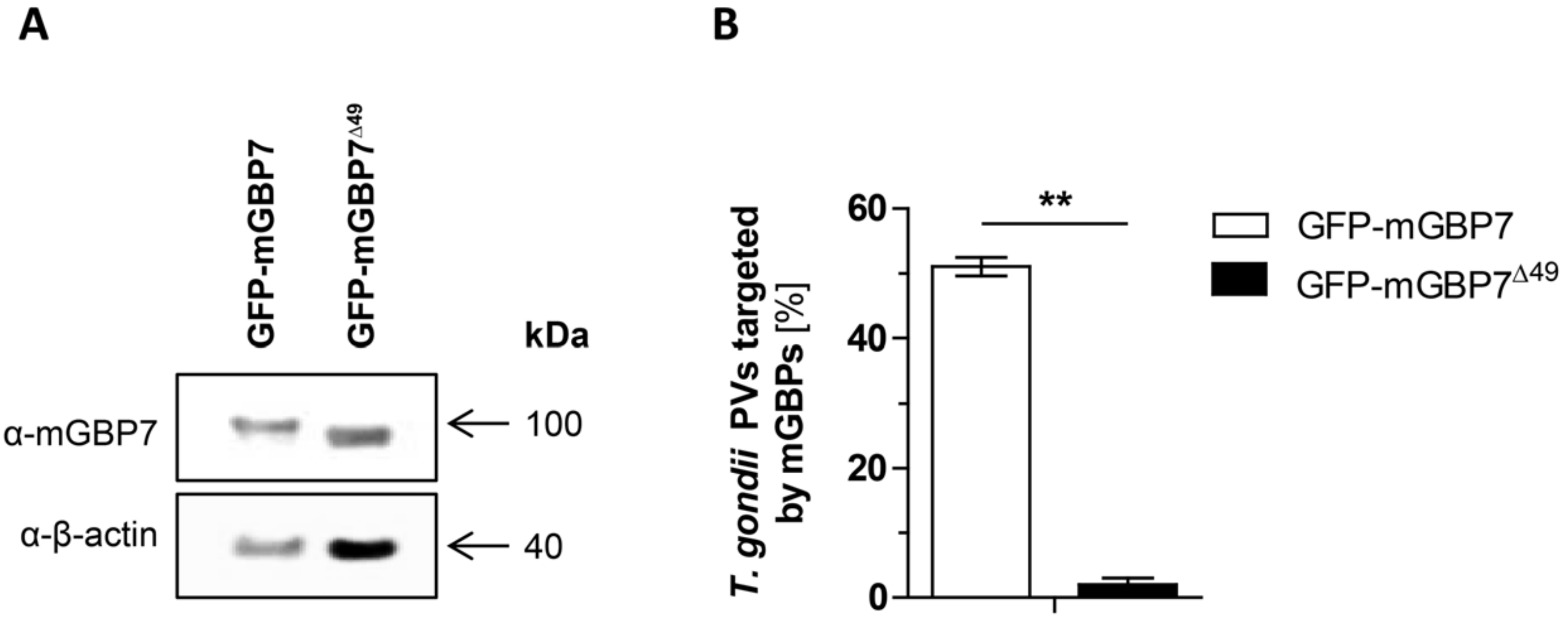
A
GFP-mGBP7
GFP-mGBP7Δ49
kDa
α-mGBP7
100
α-β-actin
40
B
T. gondii PVs targeted by mGBPs [%]
60
40
20
0
**
GFP-mGBP7
GFP-mGBP7Δ49